STRUCTURE-FUNCTION CHARACTERISATION OF FEW BLUE LIGHT RESPONSIVE PHOTORECEPTORS THROUGH BIOCHEMICAL AND BIOPHYSICAL APPROACHES.

NAME OF THE CANDIDATE: ANWESHA DEB

REGISTRATION NO : R-14RS18210031

NAME OF SUPERVISOR : Dr. DEVRANI MITRA

NAME OF THE CANDIDATE : ANWESHA DEB

NAME OF THE SUPERVISOR : DR. DEVRANI MITRA

TITLE OF THESIS : STRUCTURE-FUNCTION CHARACTERISATION OF FEW BLUE LIGHT RESPONSIVE PHOTORECEPTORS THROUGH BIOCHEMICAL AND BIOPHYSICAL APPROACHES.

REGISTRATION NO. : R-14RS18210031, 6TH MAY 2016

ENROLLMENT NO. : SC-DOC/13-14/21, 18TH JUNE 2014

PLACE OF WORK : PRESIDENCY UNIVERSITY

RESIDENTIAL ADDRESS : GA/1, NAYANMANI APARTMENT, RAJARHAT, KOLKATA-700135

CORRESPONDING ADDRESS : 6/3B, RAJWADA LAKE BLISS, SONARPUR, KOLKATA-700103

EMAIL : inca.anwesha@gmail.com

PHONE NUMBER : 7872515192

SIGNATURE OF SCHOLAR

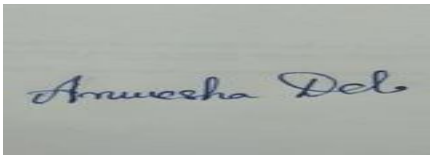

SIGNATURE OF SUPERVISOR

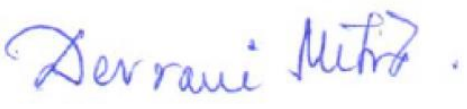

16th October 2020

CONTENTS:

ABSTRACT……...4

INTRODUCTION……..5-8

OBJECTIVES…….9

MATERIALS AND METHODS…… 9-11

RESULTS AND DISCUSSION……11-31

a. **OBJECTIVE 1……..11-16**
b. **OBJECTIVE 2……..16-28**
c. **OBJECTIVE 3…….. 28-31**

CONCLUSION……...32

APPENDIX ……33-35

REFERENCES……35-46

PLAGIARISM CERTIFICATE……...47

CONFERENCE LIST CERTIFICATE……..48-49

FIRST PAGE OF PUBLISHED PAPER……..50

ABSTRACT:

Harvesting light as the primary source of energy is one of the major phenomena behind life on earth which is mediated by several photoreceptors. Photoreceptors are critical for several physiological phenomena viz. photo-acclimatisation, phototropism, stomatal opening etc, thus making its characterisation extremely important in order to use it as optogenetic scaffold. I have been specifically interested in blue light responsive photoreceptors, found exclusively in photosynthetic stramenopile. My work primarily focuses on molecular understanding of aureochromes from two species (*Vaucheria frigida* and *Thalassiosira oceanica*) through biochemical and biophysical assays to understand its contribution towards natural phenomena or even using it to intervene in biological pathways.

1. INTRODUCTION

Light is an essential environmental cue for various physiological processes across the living world. In order to trap this light energy, the organisms harness different photoreceptors with chromophores responsive to corresponding wavelength of light[1]. Ten classes of photoreceptors discovered till date--Cryptochrome, Rhodopsin, Xanthopsin, Phytochrome, Cyanobacteriochrome, Car-H (*adenosylcobalamine containing photoreceptor*) OCP (*Orange Carotenoid Protein*), BLUF (*Blue Light Utilising FAD*), UVR8 (*UV-resistance Locus 8, a UV-B range i.e 280-320nm response pathway*) and LOV (*Light Oxygen Voltage*) proteins[2–6,5]. While the opsins absorb blue, green and red light and Phytochromes absorb far red and near infrared light, LOV, BLUF, Cryptochromes and Xanthopsins are four major classes of photoreceptors that senses UV and blue light (BL, 300nm- 500nm)[4,7]. LOV-photoreceptors are found in wide variety of organisms namely archaea, bacteria, plants, algae, fungi etc., the first being phototropin [3,8,9]which is predominantly found in plants, BL photoreceptors are also very common in marine environment because of their ability to respond to a narrow range of wavelength[10,11]. Phototropin consists of two N terminal LOV and a C terminal Serine/Threonine kinase domains--primarily responsible for phototropism and chloroplast movements [12]. Blue-green algae, red algae, diatoms are few of the photosynthetic stramenopiles that use BL photoreceptors for developmental purposes[13] .

Dark state LOV-protein binds non-covalently to a flavin (chromophore), releasing bluish green fluorescence. Upon BL absorption, reversible photo-adduct is formed between Cysteine and chromophore, resulting in loss of fluorescence. Although in most cases photo-adduct is formed by triplet state decay of FMN, in few it is also mediated by a singlet state decay e.g. in *Chlamydomonas reinhardtii*[7,12,14,15]. LOV photoreceptor exhibits a not so often coexistence of fluorescence and triplet state photochemistry, of which the former is extensively used in lab for fluorescence activities[16–22]. LOV-photoreceptors couples light responsiveness to oxygen availability, mediated by the long known flavin chromophore which can switch between its oxidative states[23,24]. They also dictate life-cycle pattern and pathway for infectivity in wide range of organisms [7]and forms an irreplaceable part of the stressosome of Ytva LOV[25–27] .

Aureochrome is one of the most recently isolated LOV protein, found exclusively in photosynthetic stramenopiles and non-existent in green plants[21,28,29] . Aureochrome, a golden yellow chromo protein was first described in the year 2007, from *Vaucheria frigida*, essential for its branching and sex-organ development[30–34]. Among the two variations found, *Vf*Aureo1 is responsible for normal branching pattern and *Vf*Aureo2 possibly for vegetative propagation.[30]

Three Aureo1 orthologs were found in *Phaeodactylum tricornutum (Pt)* --*Pt*Aureo1a, *Pt*Aureo1b and

*Pt*Aureo1c [20,32]. Both *Vf*Aureo2 and *Pt*Aureo2 lack flavin binding ability mostly function as transcription factors heterodimerizing with respective Aureo1 partners[20,32]. The diatom *Thalassiosira oceanica* was once considered same as *Thalassiosira pseudonana,* later on it was found to possess a much larger genome size of approximately 80MB [35]. Significantly large size of *T. oceanica (To)* from both of its closely related species, *Thalassiosira pseudonana*(approximately 34 MB) and *Phaeodactylum tricornutum* (approximately 28 MB) can be due to DNA recruitment from multiple sources [35]. This dissertation work primarily focuses on two different varieties of aureos - *Vf*Aureo1 and *To*Aureo1.

T. oceanica can grow in iron deficient environment although it is an important element in photosynthetic pathway [36,37] and generally found in area of low algal populations due to limited nutrient supply[38].Although initially reported in *Phaeodactylum tricornutum,* aureos are also found in other diatoms e.g. *Ectocarpus siliculosus* (Phaeophyceae), *Fucus distichus*, *Chattonella antiqua* (Raphidophyceae), *Nannochloropsis gaditana* CCMP526 (Eustigmatophyceae), *Ochromonasdanica* (Chrysophyceae), *Thalassiosira pseudonana/oceanica* (Coscinodiscophyceae)[21,28,29,31,35,39–41].

Aureochrome has diverse biological activities like controlling branching pattern and sexual propagation in *Vaucheria* to photo acclimation and photo adaptation in diatoms [30,42] in a BL-dependent manner. Upon BL absorption, photosynthetic activities of diatoms get enhanced– this is known as high light adapted state[42]. Up-regulation of several thyllakoid membrane proteins responsible for highest photosynthetic rate and presence of bZip recognition domains in their promoter region indicates their function as transcriptional regulators under BL or white light [42]. It could be confirmed by partial/complete nuclear localization of *Vf*Aureo1/2 fused with GFP [30,43]. Similarly *Pt*Aureo1, was also found to regulate cell cycle protein dsCYC2, responsible for G1 check point transition[44]. Aureochromes consist of a C-terminal LOV sensor and N-terminal DNA binding bZIP(basic Leucine Zipper)effector domain, depicting a reverse sensor-effector topology--more prevalent in eukaryotic organisms[45,46] e.g AHR-ARNT,PER-TIM, HIF[47–49].

Upon the formation of a coiled coil structure, of S/Z type plant bZIP domains[44,50–55] few peaks around P-O stretching region is illustrated by Fourier Transform Infrared (FTIR) spectroscopy on Aureo1-bZIP-target DNA complex which signify hydrogen bonding with the phosphate backbone. Additional peaks were observed at C=N and NH_3^+stretching regions, implying involvement of both Arg and Lys residues in DNA binding[56]. Absorptions in the Amide I and Amide II regions signify changes in protein backbone conformation and hydrogen bonding network which is consistent to partial unfolding of the Jα helix[44]. Homology modelling of *Vf*Aureo1 bZIP considering *S. Cerevisiae* GCN4 protein as template, shows importance of three Arg residues: Arg128, Arg130 andArg141, in binding to the target DNA [51,52]. Lys136 and Asn131 are also seen to be forming hydrogen bond with the bases[57].

LOV: a subgroup of PAS superfamily, consists of ~110 amino acid residues[58]. PAS derived its name from *Drosophila* protein Period (PER), vertebrate aryl hydrocarbon receptor nuclear translocator (ARNT) and *Drosophila* Single minded (SIM) [59–61]. LOV core adopts a typical PAS topology consisting of five anti-parallel β sheets arranged in a 2-1-5-4-3 pattern, against which the four α-helices are placed [51,62–66]. Among varieties of cofactors, like 4-hydroxycinnamic acid, Protoporphyrin IX, Flavin Adenine Dinucleotide (FAD)and Flavin Mono Nucleotide (FMN), LOV domain mostly binds to FMN/FAD[51,67–69]. LOV domain harvests light signal mostly through flavin, following which a covalent adduct is formed between the γ sulphur of a conserved Cysteine residue(generally in a sequence of GRN**C**RFLQ) and C4a atom of Flavin's Isoalloxazine ring [70,71]. The newly formed adduct results in disappearance of the peak near 450nm, and instead the peak at 390nm becomes more prominent, as observed in typical UV-Vis spectrum. Protonation at the adjacent N5 position of the isoalloxazine ring initiates signal transmission to downstream effector domains [72–76].Even in absence of active site Cysteine, LOV has been found to trigger downstream signaling to neutral semiquinone state when N5 is protonated – as found in recent evidences[16,77–84]N5 protonation allows the conserved Glutamine to flip its amide side chain by $180^0$and change the existing set of hydrogen bonding network. This disruption in network passes through the LOV core domain to the flanking N and C terminal regions, placed against the LOV core[63,77,85–88]. The photo-adduct formation is always reversible and comes back to its non-covalently bound state spontaneously. However, the dark reversal time varies from seconds to hours. However, mutations in specific residues can create constitutively light/dark adapted protein. The conserved Cysteine, if mutated to Alanine, locks the protein to a permanent dark adapted state. Again, a certain conserved Gln when mutated to Asn, lit state is favoured[89]. Further, fine temporal control on the bZIP domain might be achieved by mutating specific residues in the LOV domain, responsible in changing the dark recovery kinetics. For example in VVD, mutation in Isoleucine residues (74,85) altered its dark recover kinetics significantly[70]. For thorough understanding of dark reversal at the residue level a theoretical approach can be taken in the form of Residue Interaction Network/Graph (RIN/RIG)[90]

The method can be used to see a change in pattern of long distance signal transduction within the protein, especially when the structural changes are not very prominent in crystal structures[90]. Network calculation [91,92]is based on graph theory, evolution of which started back in the year 1975[93–96]. RIG, also known as Protein Contact Network (PCN), along with differential network (DN) has the potential to identify the residues important for the change in signalling pattern, e.g. dark light transition[90]. This approach not only helps in temporal control of the LOV protein (i.e change in light adapted state life time of the protein) but also spatial control of the same, by taking an informed decision regarding the type of LOV variant and the effector to which it is connected. Ability to attain such spatio-temporal control of modular LOV containing protein is indeed beneficial in designing artificial photoreceptors suitable for optogenetics[97].

First in 2005, microbial opsin was introduced to make the neurons light responsive and optogenetics was developed[98–101] followed by implementation of channel-rhodopsin, bacteriorhodopsin and halorhodopsins. The hurdle to optogenetics implementation deep inside the tissue was removed by fiberoptic and laser-diode tools [102,103]. Its applications became wide spread with extensive study of several other photoreceptors like LOV, Cry, Phy, which could target diverse cellular functions[5]. Reversibility and modularity are critical to a photoreceptor for being an optogenetic tool. Several optogenetics systems are designed using modular LOV-photoreceptors as sensors [5]. E.g. LOV-TAP chimera uses LOV2 domain of *Avena sativa* phototropin1 (*As*LOV2)fused with the *Escherichia coli* TrpR, while *As*LOV2 fused to Rac1 generates blue light sensitive RAC-GTP*ase* [104,105]. YtvA LOV (*Bacillus subtilis)* when fused with FixL Histidine kinase (*Bradyrhizobium japonicum),* two component system FixL-FixJ got light sensitive[65]. While linker region of LOV photoreceptors are critical in transmission of signal to the effector domain, standalone photoreceptor like VVD (Vivid) has been used to generate light activated magnets having oppositely charged dimerization interface[106]. Few other criteria for designing optogenetic tools are choice, efficiency and abundance of chromophore, conformational changes in the target protein with photon absorption and most importantly, achievable spatio-temporal control over diverse cellular mechanisms [5,107–111]. *AsLOV2* is among the most frequently used scaffolds (87%)[102,104,120–129,112,130–138,113–119] in LOV based designs. The uniqueness of *As*LOV2 lies in a distinct phenomenon of Jα detachment from the LOV core, upon BL illumination[5,112,139]– first observed by Harper *et al*.[33,72]. Flipping of a Gln residue, located at Iβ, upon photo excitation is believed to be critical in signal transmission from sensor to effector via linker[63,140–143]. Changes in the hydrogen bonding pattern results in unfolding of Jα and further effector functioning[72,139]. With detailed mechanistic insights available, *As*LOV2 has become a favourite sensor module for photoreceptor-engineering and designing constructs for optogenetics.

This study focuses on structural and functional characterization of aureochromes (especially *To*Aureo1 and *Vf*Aureo1) and explores the possibility of using them in optogenetics.

2. Objectives:

- Structural characterization of Aureochromes (AuLOV, AubZL etc.), especially from *Thallassiosira sp*. through spectroscopy and theoretical studies.
- Modulation of life cycle of LOV sensor domains in Aureochromes through kinetic characterization.
- Structure-guided design of optogenetic scaffold from Aureochromes.

3. Materials and Methods:

3.1 **Cloning and expression:** Aureochrome1 genes of *Thalassiosira* (*To*Aureo1) were ordered from *GeneArt Strings* from *Invitrogen* and that of *Vf*Aureo1 was a kind gift from Keith Moffat's laboratory at The University of Chicago. The codon optimized genes are cloned into pET28a vector at Nhe1-Sac1 and BamH1-Sac1 sites respectively and transformed in DH5α for amplification. This is followed by plasmid isolation using *Promega plasmid isolation miniprep* kit and validation through DNA sequencing (*Eurofins Genomics India Pvt. Ltd.*) The plasmid DNA bearing Kanamycin resistance marker, is next transformed into BL21-DE3 and BL21-C43 cells, which we received as a gift from Dr. Jayanta Mukhopadhyay's laboratory at Bose Institute, Kolkata. Colonies obtained are further expressed in large cultures (2-4 litres) using IPTG (300uM) (*Isopropyl β- D-1-thiogalactopyranoside*) for 12-16 hours at 20-22°C.

3.2 **Site directed mutagenesis:** Mutation primers are designed using WT (*wild type*) plasmid *Vf*Aureo1LOV as template. Mutagenesis PCR, using standard protocols from *Stratagene* is followed in which 4 hours of Dpn1 digestion is followed by PCR purification, which DH5α cells. The colonies are screened and correct identified and by DNA sequencing (*Eurofins Genomics India Pvt Ltd)*. Each plasmid DNA bearing the desired mutation(s) is subsequently expressed in BL21 DE3/DE3 (C43) as mentioned above.

3.3 **Protein purification:** IPTG induced *E. coli* cells bearing plasmid DNA are harvested (8000 rpm for 10 minutes) and the supernatant is discarded. The pellet thus collected is next treated with lysis buffer (*20mM Tris, pH 8; 50mM NaCl; 10% glycerol*), followed by sonication and high speed centrifugation at 14000rpm for 1 hour. The supernatant is then passed through Ni-NTA column (*Qiagen*) followed by a wash buffer (*20mM Tris, pH 8; 50mM NaCl; 10% glycerol, 50mM imidazole*) and finally elution buffer (*20mM Tris, pH 8; 50mM NaCl; 10% glycerol, 250mM imidazole*). The elute collected in multiple fractions are concentrated to 2.5ml and passed through PD10 desalting column (*Thermo Scientific*) to get rid of excess imidazole. The elute is collected in lysis buffer (*20mM Tris, pH 8; 50mM NaCl; 10% glycerol*).

3.4 **Size exclusion chromatography:** While the mutants of Objective 2 are passed through desalting columns, protein samples prepared for Circular Dichroism (CD) or Electrophoretic Mobility Shift Assays (EMSA) are passed through size exclusion chromatography column (*Bio-rad)* in order to separate the monomer from dimer. The eluted fractions from affinity chromatography are first concentrated to 500µl and injected onto the Bio-rad column. The column was pre-equilibrated with lysis buffer (details above)

using a Fast Protein Liquid Chromatography (FPLC) system (*Bio-rad, Biologic DuoFlow*). Fractions containing dimers, as selected through the observation of elution profile, are collected and concentrated using Amicon centrifugal concentrators (*Millipore*). The purified samples containing 10% glycerol are either used immediately or stored at -20^{0}C until further use with necessary photo-protection.

3.5 **UV-Visible Spectroscopy:** The purified protein sample is subjected to UV-Visible scanning from 230nm to 700nm. The protein is then exposed for 10-15 minutes of bright white light (364W/m^2), as applicable for different samples. Dark recovery kinetics is conducted till the native dark spectrum is generated. The optical density (OD) against 447nm (OD_{447}) is then plotted against time (*in seconds*) to calculate the rate constant (k) for a single exponential equation in which $OD_{447} = constant(1- e^{-kt})$.

3.6 **Circular dichroism spectroscopy:** The concentration of the purified protein samples is adjusted to 15µg/ml - 25µg/ml. The proteins considered for CD spectroscopy are *To*bz (bZIP+LOV of *To*Aureo1) and *AsTo*bz (fusion protein of *Avena sativa* and *Thallassiosira oceanica* LOV2 and bZIP respectively). Data for both dark and light adapted state of the proteins are recorded, the average of which are plotted against wavelength and analysed through BeStSel application.

3.7***In silico*** **modelling and docking:** In absence of experimental structure, the sequence of *To*Aureo1 subjected to homology modelling using *DiscoveryStudio* and *SwissModel*. With no homology observed against the linker region connecting bZIP and LOV, both these domains are modelled individually. The LOV domain of *To*Aureo1 was modelled using *DiscoveryStudio* along with the FMN as cofactor[144]. The bZIP is found to be structurally similar to PDB entry 1DH3 (crystal structure for CREB binding protein from *Mus musculus*) and is therefore used for *To*Aureo1-bZIP homology modelling[145]. Both the structures are energy minimized using Chimera after a Ramachandran analysis using *Molprobity* option of SwissModel [146]. Post energy minimization Ramachandran analysis is done using Procheck and finally docked with 21bp CRE DNA from 1DH3 crystal structure using NPDock. The docked protein models are analyzed using PyMol visualization program.

3.8**Electrophoretic Mobility Shift Assay:** EMSA is carried out to study DNA-binding activity of *To*bz and *AsTo*bz. A 24 bp DNA fragment [5′d(TGTAGCGTCTGACGTGGTTCCCAC) 3′ and complementary sequence] containing the consensus CREB binding site, TGACGT, were synthesized from Integrated DNA Technologies (IDT). Lyophilized DNA strands re suspended in nuclease free water and 10µM from each annealed by rapid heating at 95°C followed by gradual cooling in annealing buffer (*12 mM Tris; pH 8.0, 30 mM NaCl*). A final concentration of 0.5µM double stranded DNA (dsDNA) is used in the

assay buffer (*50mM Tris; pH 8.0, 20mM NaCl, 0.5mM DNA, 1.25mM $MgCl_2$, 20% Glycerol*). Serially diluted protein is then added to the reaction mixture and incubated at 22°C for 1hr. Along with the protein-DNA complex, control (free DNA) set are resolved in 10% polyacrylamide gels at 180V for 35 minutes. The gel is then stained with SyBr Gold (Thermo Scientific) in 0.5X TBE buffer (Tris Borate EDTA) for 40 minutes and image is taken by gel documentation system (*Chemidoc, Bio-rad*).

3.9Screw axis rotation: For Differential Network (DN) approach to study dark light transition of LOV domain *Vaucheria frigida* Aureochrome (*Vf*Aureo1) crystal structures (3UE6 and 3ULF) were taken initially, although later on crystal structures (5DKL and 5A8B) of *Phaeodactylum tricornutum* aureochrome (*Pt*Aureo1) were considered to determine the relative orientation of the monomers by rigid body screw axis rotation analysis using Isqkab [147] and CCP4 suite. The magnitude of screw-rotation (expressed as ρ in degrees) and translation (d in Å) is determined, superimposing the initially non superimposed monomeric units for the Cα atom, after the monomers of dimeric VfAureo1 dark and VfAureo1 light are superimposed using Cα least square fit analysis. To mimic the anti-parallel orientation of *Pt*Aureo1, *Vf*Aureo1monomers are translated and rotated using PyMol.

4. Results and Discussion:

4.1Objective1: Structural characterisation of *To*Aureo1 is carried out through spectroscopic and theoretical studies. Both LOV domain of *To*Aureo1 (*To*AuL) and bZIP+LOV domain of *To*Aureo1 (*To*AubZL) are purified using above-mentioned procedures. Purified protein fractions are verified by SDS-PAGE and concentrations are measured using OD_{447nm} with extinction coefficient of 12,500 $M^{-1}cm^{-1}$.[51]The rate constants for dark-recovery kinetics are then calculated following their measurements in UV-Vis spectroscopy (Fig:1.1).

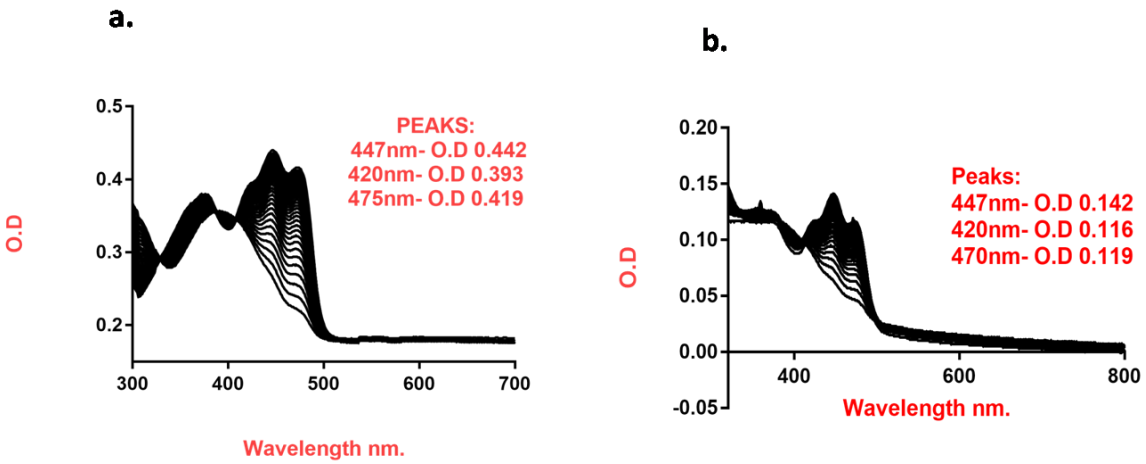

Figure 1.1: a.*To*AuL dark recovery kinetics b. *To*AubZL dark recovery kinetics .

VARIANT	RATE CONSTANT ($s^{-1}\pm10^{-5}$)	LIFE TIME
*To*AuL	2.2 x10^{-3}	38.5 minutes
*To*AubZL	2.04 x10^{-3}	35 minutes

TABLE 1: Rate constant and life time of ToAubZL

With no homology found against the linker region, both LOV and bZIP domains are modeled separately (Fig:1.2). The best model of *To*AuL as predicted by DiscoveryStudio taking 1N9L as target PDB, showed 1.33 clash score (ideal ≤ 0.4), Ramachandran favored 97.8% (ideal >98%) , rotamer outliers 1.20% , C_β deviation score 2 (ideal ≤ 0.25)in Molprobity. Therefore, energy minimization is performed using Chimera [148]. Energy minimized structure gave us a clash score of 0.7%, 100% Ramachandran favored structure, and 0 score against both C_β deviation and rotamer outliers, thus providing a satisfactory model of *To*AuL. The preceding bZIP domain was modelled against 1DH3 and analysed using Molprobity which showed a clash score of 0.70, 100% Ramachandran favoured structured and 0.0% rotamer outliers. After energy minimization of the structure using Chimera the clash score reduced to 0.59, along with 100% Ramachandran favoured structure and 0 score against rotamer outliers.

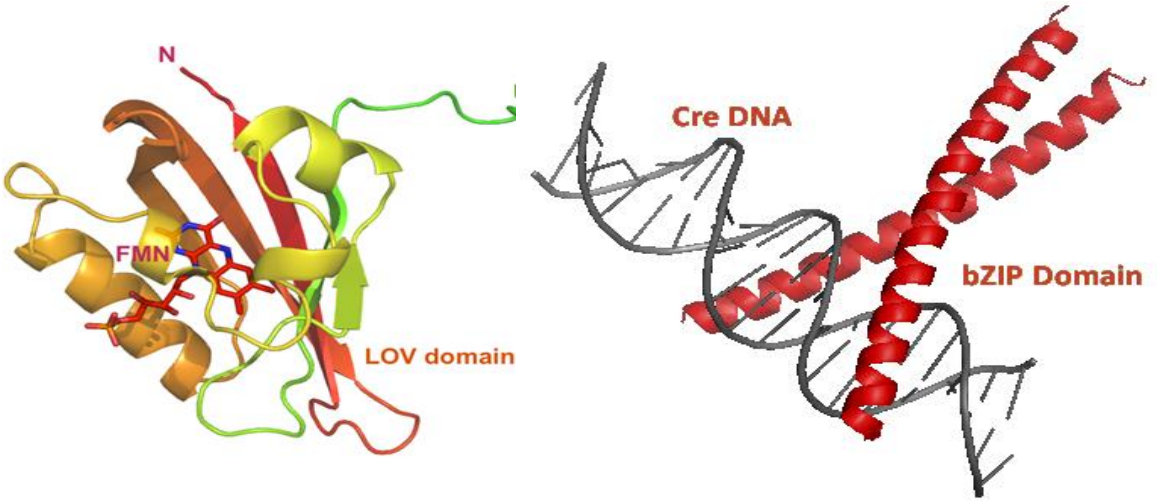

Fig 1.2: *To*AuL domain docked with FMN and TobZIP domain docked with cognate DNA.

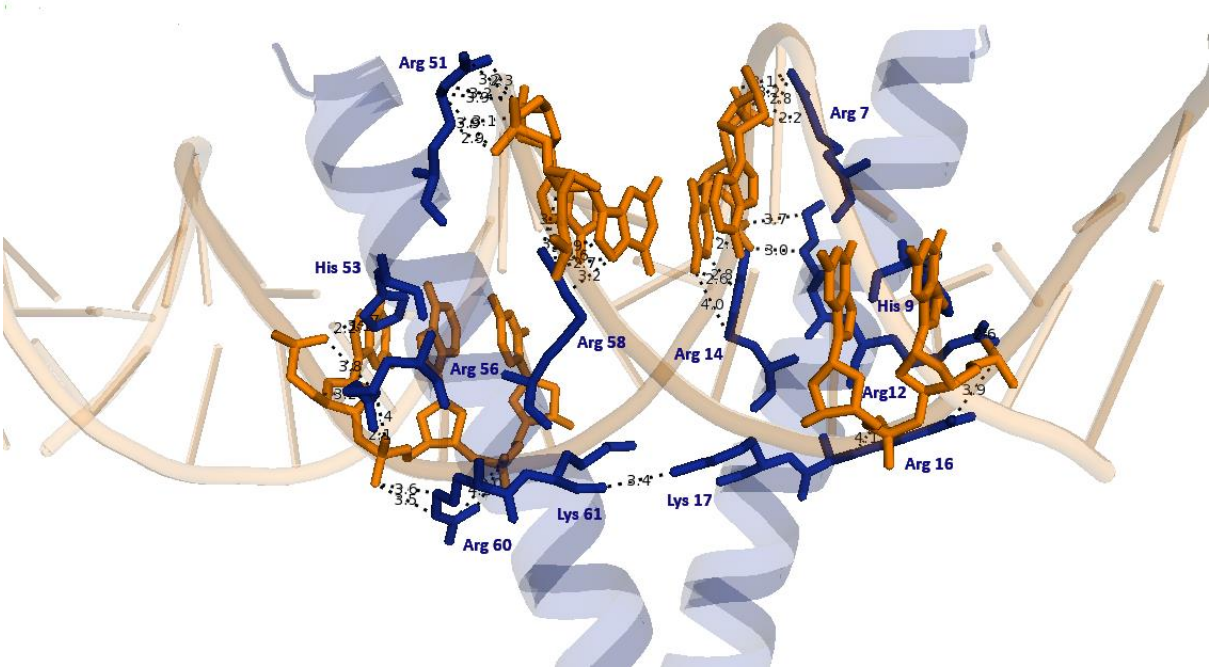

Fig 1.3: *To*bZIP docked to the Cre DNA and few interactions with conserved amino acid residues present in all Cre-Binding Proteins.

bZIP+LOV of *Vf*Aureo1 when subjected to sequence alignment to *To*AubZL revealed that, they have a perfect similarity to each other with respect to the basic DNA binding region of the bZIP domain (Fig:1.3). Hence it was deduced that *To*AubZL could be Cre (ACGT) binding protein as well[51].

```
VfAureo1        EAQKVERRERNREHAKRSRVRKKFLLESLQQSVNELNHENNCLKESIREHLGPRGDSLIA 180
ToAubZL         ------RRERNREHAKRSRIRKKFLLESLQQSVSLLKEENGKLKNAIRTHLGEKE----- 49
                      *************:*************. *:.**. **::** *** :
```

Fig 1.4: Sequence alignment of *Vf*Aureo1 with *To*AubZL

Then a multiple sequence alignment was done using Cre binding Proteins.

```
ATF5            KRDQNKT-AAHRYRQRKRAELDSLEEQLHCLEGRNRELRDK--------AESVEREIQYV
Atf2_tp         RLEQNRR-AAVESRRRKKIKEAELQRSFDHYTKTNHSLSMQ--------NHELEKQILLA
AtfA            FLERNRV-AALKCRQRKKQWLANLQAKVELFTSENDALTTT--------VTQLREEIVNL
ATF3            RRERNKI-AAAKCRNKKKEKTECLQKESEKLESVNAELKAQ--------IEELKNEKQHL
To_bZip         RRERNRE-HAKRSRIRKKFLLESLQQSVSLLKEENGKLKNA--------IRTHLGEKE--
                    Nxx-AAxxCR
```

Fig 1.5: Sequence alignment of Cre Binding Proteins.Cyclic AMP-dependent transcription factor 2 (Atf 2), Activating transcription factor A(Atf A), Cyclic AMP-dependent transcription factor 3(Atf 3), *Thalassiosira oceanica* bZIP (*To*_bZip)The signature sequence 'NxxAAxxcR' is conserved in To_bZIP present in Cre binding bZIP.

With strong predictions for Cre-sequence binding ability, EMSA was performed with *To*AubZL using two sets of oligo-nucleotides having ACGT motifs.

EMSA_Cre_bZIP_1: 5′TGT CCT TGG CTG ACG TCA GCC AAG CAC 3′

EMSA_Cre_bZIP 2: 5′TGT AGC GTC TGA CGT GGT TCC CAC 3′

Basic region of bZIP domain of *To*AubZL was mutated to change its specificity to the EMSA_Cre_bZIP_1 DNA. In the first variation (V1) His310 was mutated to Ser and Lys312 to Ala, while in the second variation (V2) Histidine was mutated to Serine and Lysine to Leucine.

***ToAubZL*:** 5′ RRERNREHAKRSRIRKKFLLESLQQSVSLLKEENGKLKNAIRTHLGEKE 3′

V1 :5′ RRERNRESAARSRIRKKFLLESLQQSVSLLKEENGKLKNAIRTHLGEKE 3′

V2 :5′ RRERNRESALRSRIRKKFLLESLQQSVSLLKEENGKLKNAIRTHLGEKE 3′

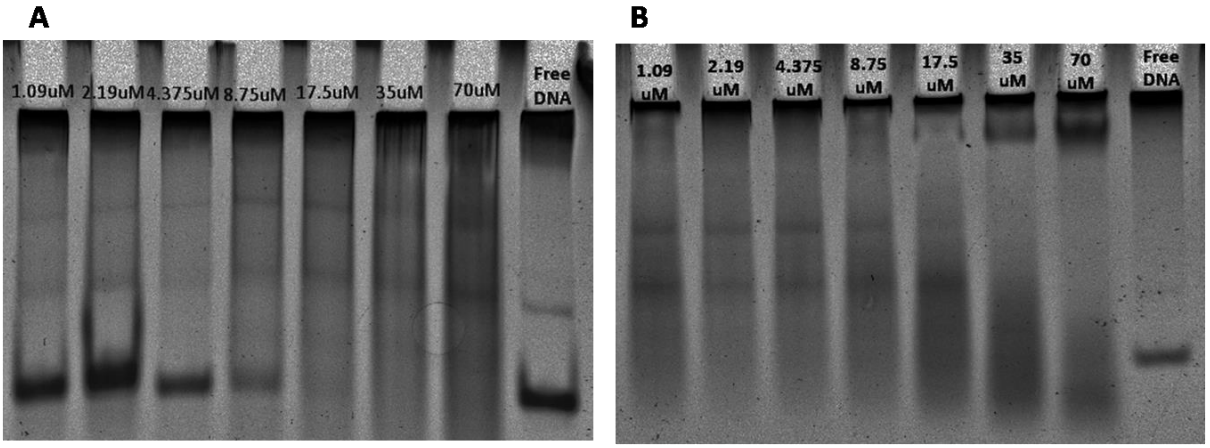

Fig 1.6: a. EMSA of *To*AubZL(WT) in dark, b. EMSA of *To*AubZL in light.

In the above gel we can see free DNA from 3.75uM concentration of protein in dark but in lit condition no such free DNA appears for the same concentration of protein (Fig:1.6).

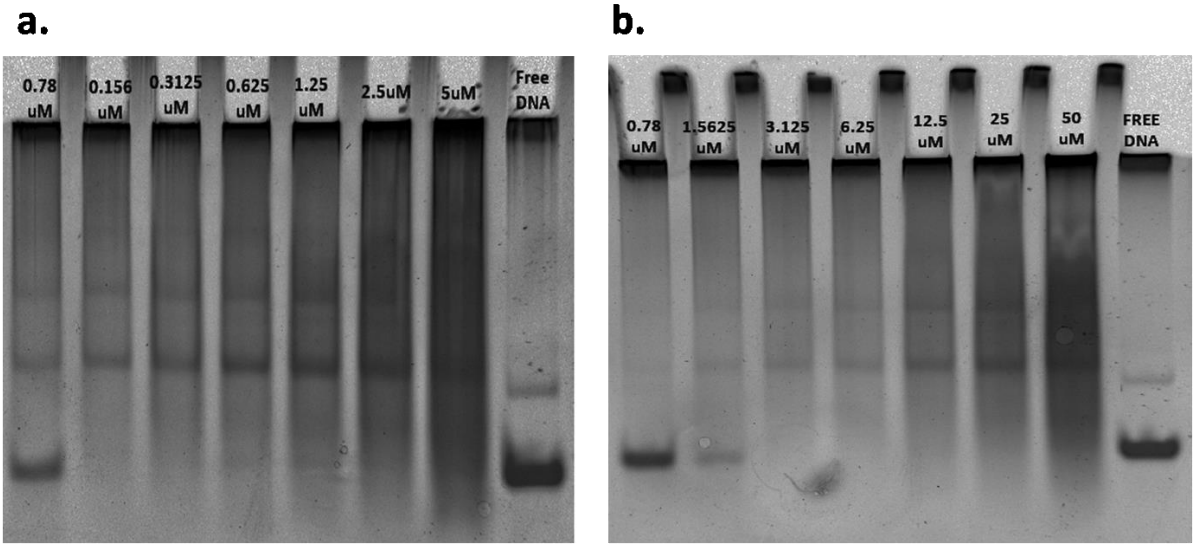

Fig 1.7: Figure a and b shows EMSA of V1 and V2 with cognate DNA in constant light.

In case of V1 and V2, EMSA was performed under constant light conditions with a change in the basic region of the bZIP. It is observed that V1 is 10 times more efficient in DNA binding compared to V2 for the same amount of DNA (Fig:1.7). The above experiment has been repeated multiple times with same resul .

4.2 Objective 2: Under second objective we focus on modulation of light-state lifetime of LOV sensor domain from Aureochromes, through kinetic characterization. *Vf*Aureo1 LOV has been used for conducting the experiments. LOV photoreceptors possess a reasonably conserved amino acid sequences, stable under evolutionary selection pressure. Therefore, LOV photoreceptors are widespread and serve diverse biological functions. However, subtle changes in specific amino acid positions can hugely affect dark reversal kinetics. Alteration of kinetic parameters like light state lifetime is not only physiologically significant but also important in generating temporal controls for optogenetics. Differences in light versus dark structures are not very prominent except in few amino acid positions. To address this, differential network (DN) approach was proposed by Dr. Soumen Roy's lab to identify residues that undergo changes during light→dark transition [90]. There is a challenge in calculation of RIG which requires simultaneous availability of crystal structures at both light and dark states, preferably from identical crystal forms [149]. This criterion was met with dark (3UE6) and light state (3ULF) LOV structures of *Vf*Aureo1 and RIG+DN were calculated. By calculating the effect of 'edge removal' on several network metrices like closeness/betweenness centrality, edge proximity etc. important residues for light-dark transition were predicted.

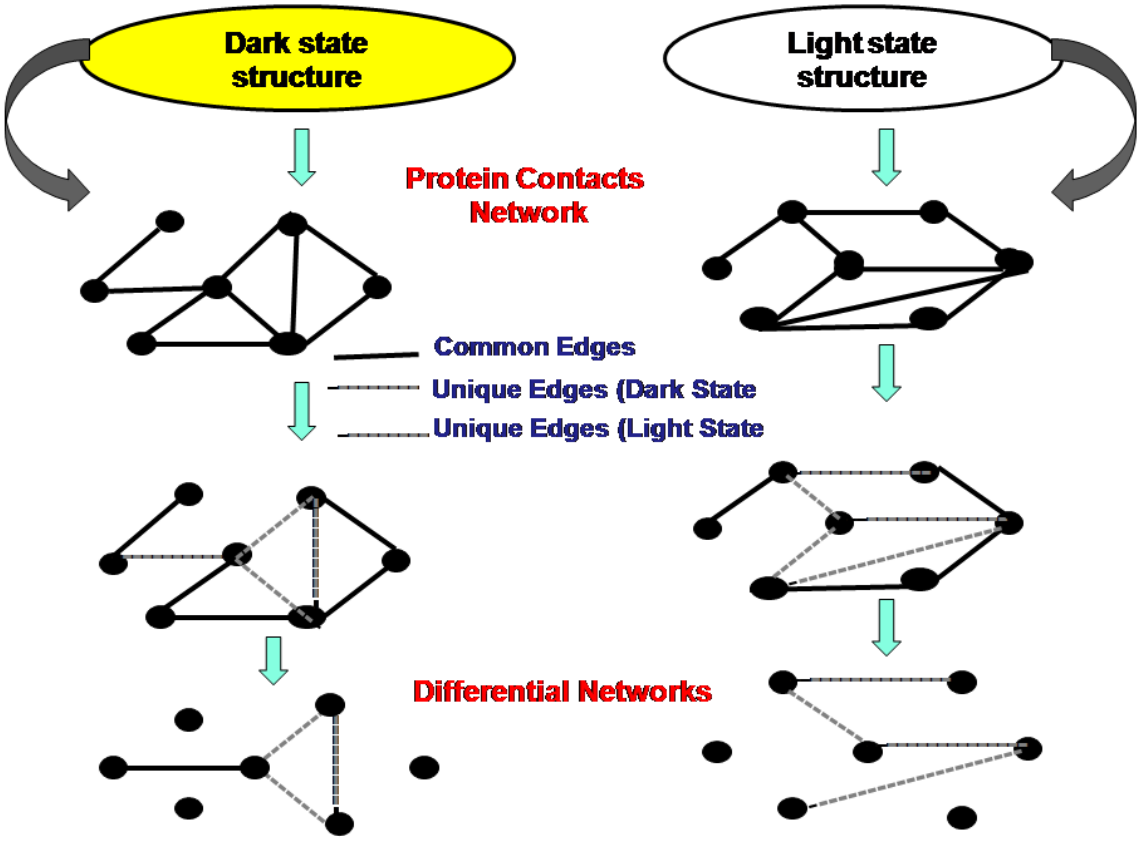

Fig 2.1: Schematic representation of Residue Interaction Graph (RIG) and construction of Differential Network (DN)

Construction of DN considers unique edges in dark and light state crystal structures. While DDN considers unique edges (amino acid interactions) in dark state, LDN accounts for the unique edges in the light state structure. The next challenge after mapping the important edges was to implement the findings from DN analysis through experiments. Before proceeding with the experiments few edge deletion models and interaction strength.

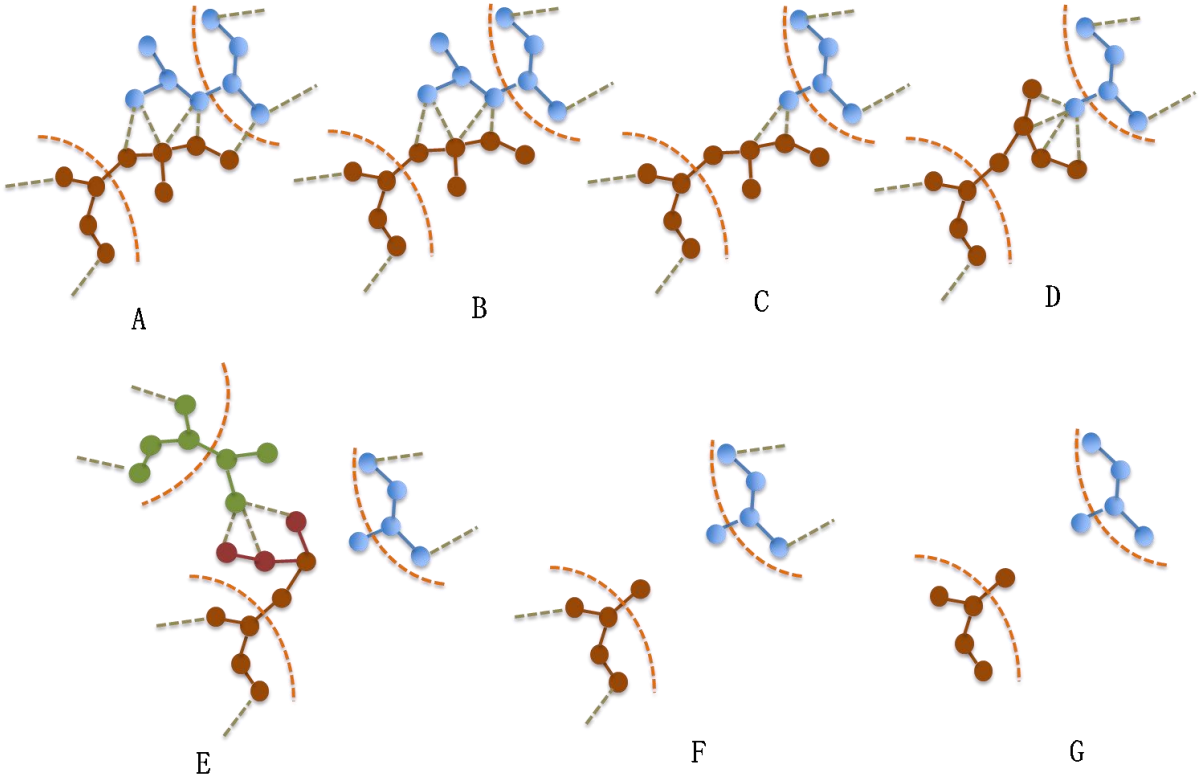

149

Fig 2.2: Several models showing different number of interacting atoms (maroon and blue) in a pair of amino acid residues having Interaction strength I_{ij}= n_{ij}/sqrt(Ni*Nj), where $n_{ij}$is number of interaction (edges) between residue "i" and "j", N_i and N_j are the number of residues in residues " i" and "j". A. Interaction between both backbone and side chain residues where I=0.7, B. Interaction between only side chain atom where I= 0.6. Number of edges in B, being more feasible than in case of A, former is considered as wild type (WT) model for RIG interaction. C. Number of side chains are reduced like Alanine scanning mutagenesis showing I=0.3 which is half of 0.6. D. Variant of B, keeping the number of interactions same even after mutation. E. The edge between residues of interest become I=0 after mutation of one residue, instead forming edges with a new residue in green. F. This is a perfect model of mutation where I=0, after double mutation and without any neighbourhood interference. G. This is the only model where nodes (amino acid residues) are completely deleted having I=0,but also deleting the backbone, which is practically not possible. Therefore reducing the edges was found to be more feasible approach; hence reduction of 'I' was attempted by inducing mutation in residue pairs identified by LDN and DDN.

Understandably, residue alteration is never easy especially when the choice could be made from nineteen possible candidates. Keeping Alanine scanning mutagenesis in mind, mutations were performed both at

single amino acid position as well as in pairs. Following purification of each mutants and UV-Vis spectroscopy was conducted. The changes in UV-Vis spectroscopy are depicted in Table 3 and Figure 2.3.

Mutants of Aureochrome1 LOV from *Vaucheria frigida*	**Rate constants from dark recovery kinetics (s^{-1}) ($\pm 1x10^{-6}$)**	**Lifetime (s), comments**
Wild type	$2.3x10^{-3}$	475
I270M_I274V	1.8×10^{-3}	693
I274V	$3.0x10^{-3}$	546
I270M*	$6.2x10^{-3}$	1620, prolonged light state
C283A_Q332A	$2.8x10^{-3}$	496
Q332A	$1.5x10^{-3}$	578
P204A_L212P	$4.1x10^{-3}$	365
P204A	$1.5x10^{-3}$	630
V209A_V314A	$4.1x10^{-3}$	420
V209A	$1.5x10^{-3}$	578
T262A_L284A	$1.3x10^{-3}$	693
L284A	$1.3x10^{-3}$	693
K269A_V282A	$8.8x10^{-4}$	1066, prolonged light state
V282A	$1.6x10^{-3}$	770
Y244F_L257I	$2.3x10^{-3}$	Deviation from typical LOV spectra
Y244F	$2.5x10^{-3}$	462
A266E_L284A	$1.4x10^{-3}$	Deviation from typical LOV spectra
A266E	$2.7x10^{-3}$	257
Q258A-N286A	----------	FMN binding fully compromised
Q258A	$2.5x10^{-3}$	Poor FMN binding
N286A	----------	FMN binding fully compromised
L284A_F298A	----------	FMN binding fully compromised

F298A	$2.6x10^{-3}$	4080, prolonged light state

Table 2: Parametres of dark recovery kinetics of VfAureo1 LOV mutants.

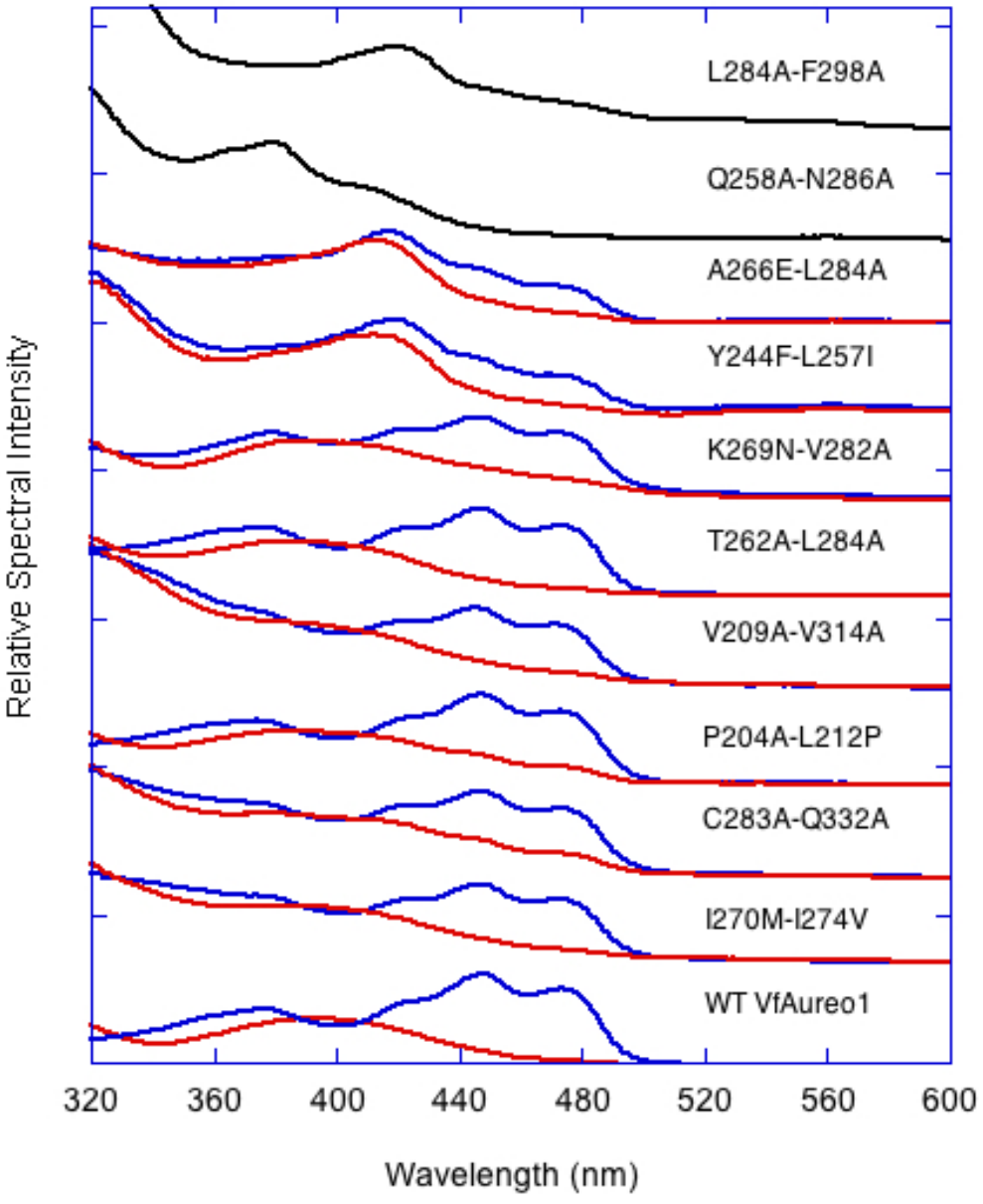

149

Fig 2.3: UV_Vis spectra of both wild type and mutants are shown in Blue (dark) and Red (light). The dark spectra show a peak at 447 nm, but it is flattened on photo bleaching. For better comparison the spectra are brought to same scale. Double mutants (Leu284Ala-Phe298Ala and Gln258Ala_Asn286Ala) are depicted by black line because they remain unchanged in light and dark. Typical dark state spectrum is missing for Ala266Glu-Leu284Ala and Tyr244Phe-Leu257Ile.

Leu284Ala_Phe298Ala failed to show typical dark-state spectrum with no absorption at 447nm (Fig:2.3). Instead, an absorption maxima is seen at 420nm. Although Phe298Ala alone is capable of yielding typical LOV dark-state spectrum*Vf*Aureo1 albeit with a prolonged life time[51], mutation in the homologous position in *As*LOV2causes improper protein expression[149,150]. Crystal structure of *Vf*Aureo1 shows an orchestrated movement of Phe298 and Leu284 upon photon absorption, with Leu284 maintaining crucial contacts with

Asn296 and Asn286.

Gln258Ala_Asn286Ala edge deletion representing model F of Figure 2.2, disrupts LOV photocycle significantly, and is unable to produce the typical spectrum (Fig:2.3). Position of Asn286 and Asn296 are homologous to Asn94 and Asn104 of Ytva, substitution of which leads to altered LOV photocycle spectrum and kinetics [151]. Gln258 is altered to Ala similar to model C of Figure 2.2, which might not have changed the FMN binding environment on contrary to Asn286; hence retaining the WT LOV spectra.

Ala266Glu_Leu284Ala and Tyr244Phe_Leu257Ile show WT like dark-state spectrum (Fig 2.3), with a comparatively weaker peak at 447nm and 475nm. However, these failed to go back to the original dark spectrum even after continuation of data collection for 100 and 50 minutes respectively (against normal 20-30 minutes). Ala266_Leu284 is a key interaction and Tyr244_Leu257 has high centrality values. According to network theory, disruption of edges possessing high centrality values could completely disrupt LOV photocycle.

In DN analysis, disruption of edge between Lys269_Val282 resulted in drastic changes in network parameters. Upon experimental investigation, a notable decrease in the rate of dark recovery is observed [Table3]. Critical for Fα-Gβ interaction, single mutant Lys269Asn not only abolishes the interaction between these Lys269 and Val282 but also eliminates Val282's interaction with Ile270 (Figure 2.4E). Further, Fα-Jα connection is abolished as hydrogen bonds between Lys269-Glu335 and Lys269-Tyr336 are lost.

Thr262 is predicted by network theory as a key residue in high edge proximity analysis. Further, Thr262 is mostly conserved across several LOV species (except ZTL,LKP2,FKF1 where it is substituted by Val).This residue is important for the stabilisation of loop structure between Eα and Fα (Figure 2.4F)[152]. Mutations of Thr262 and Leu284 to Ala make them distant, but, other interactions remaining intact, no apparent change in dark recovery kinetics or spectra is observed (Figure 2.2) [Table 3].

Gln332 of Jα and Cys283 of Gβ forms an edge in dark differential network (DDN), deletion of which could be achieved by mutating both to Ala. They resemble interaction models C and F (Figure 2.2) respectively. Double mutation causes disruption of Gln332-Val282 interaction, while rest of the interactions remain intact (Figure 2.4G). Although Jα–Gβ stabilisation is disturbed, but is possibly balanced by interaction between Glu335/Tyr336-Lys269 interactions.

Another interaction involves Ile270 and Ile274, of which Ile270 is almost conserved except for Met135 in VVD and Ile274 is often substituted with Val or Leu. On BL absorption there is an adduct formation

followed by a tilt in the planarity of flavin ring because of its sp^3 hybridization. This results in steric clash of flavin re-face thus emphasizing its importance in LOV maintaining adduct state stability and light state lifetime [85,153]. Both Ile270 and Phe298 are present in this re-face, alteration of which leads to slower dark-state recovery. In WT when Phe298 and Leu284 undergoes an orchestrated rotation, Ile270 also rotates slightly to maintain its contact with Leu284 (<0.4 Å).When Ile270 is mutated to Met, it still remains within Vander waal radius with Leu284 (Figure 2.4H), though creates a steric hindrance to Phe298. Ile274, when mutated to Val, fails to make contact with Met270[149].

The last two pairs of interactions shown in Table3 Val309-Val314 (Figure 2.4I) and Pro204-Leu212 (Figure 2.4J) are present at the interface of LOV dimer. The crystal structures of *Vf*Aureo1 LOV (3UE6/3ULF) are anti-parallel dimers unlike the biologically appropriate parallel dimer. According to recent reports[5], construction of RIG is essentially dependent on the experimental 3D structures. Therefore, presence of crystallographic artefacts (conflict between parallel and anti-parallel dimers) could automatically creep in RIG. For *Pt*Aureo1 the crystals were grown under constant light and produced biologically active parallel dimer[154]. That raised a question -- whether the residue pairs at interface would still be shown as critical edges in RIG calculations, if *Vf*Aureo1 LOV was solved as parallel dimers.

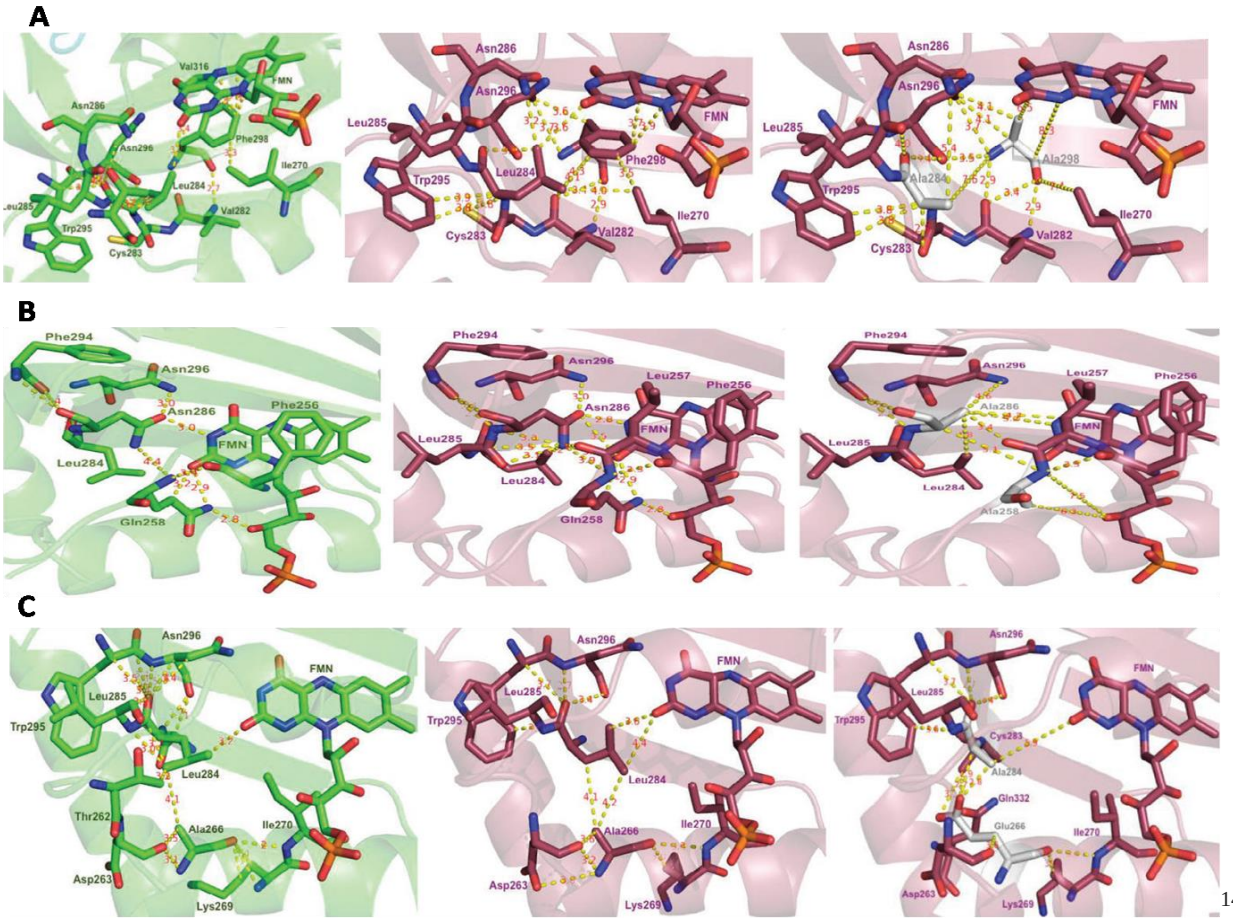

149

Figure 2.4: Pictorial depiction of amino acid residue of *Vf*Aureo1 and their edges found important in Dark and lit-state structures. *From left to right*: Panel 1 shows important residues of dark structure, Panel 2 shows important residues and their interactions in lit-state structures, Panel 3 shows changes in interaction after double mutation. The last two pairs are not shown separately because they lie in the interface and are thought to be biologically irrelevant due to antiparallel nature of 3UE6/3ULF.

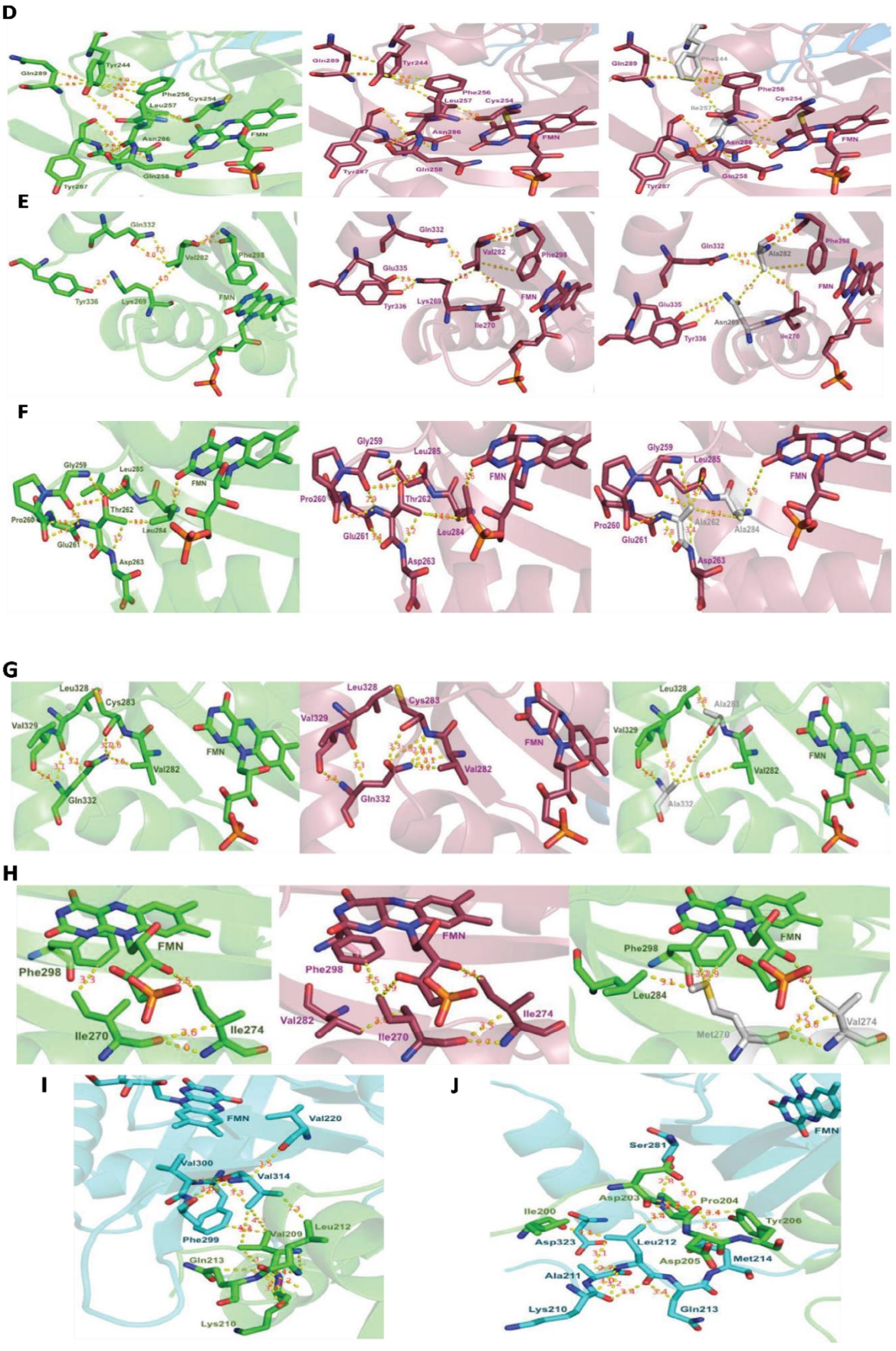
D
Gln289
Tyr244
Phe256
Cys254
Leu257
Asn286
FMN
Tyr287
Gln258
E
Gln332
Val282
Phe298
Tyr336
Lys269
Glu335
Ile270
Asn269
Ala282
F
Gly259
Leu285
Pro260
Thr262
Glu261
Leu284
Asp263
Ala262
Ala284
G
Leu328
Cys283
Val329
Val282
Gln332
Ala283
Ala332
H
Ile270
Ile274
Val282
Leu284
Met270
Val274
I
Val220
Val300
Val314
Phe299
Val209
Leu212
Gln213
Lys210
J
Ser281
Asp203
Pro204
Ile200
Tyr206
Asp323
Asp205
Met214
Ala211

Figure 2.4(continued)

In an attempt to remove such crystallographic artefacts, a notion of quaternary structural alignment is adopted in the *Vf*Aureo1 structure[51] which can remove the anomaly in residue interaction interface caused due to non-biological dimerization . For this purpose, *Pt*Aureo lit-state (5DKL) and dark state (5A8B) crystal structures were taken as references[154,155]. 3UE6 was first separated into monomeric units and aligned to a single unit of 5A8B, while another monomeric unit of 3UE6 is rotated and translated to be in alignment of another unit of 5A8B. Light-state structure of *Vf*Aureo1 (3ULF) is similarly aligned with 5DKL, to generate parallel dimer of *Vf*Aureo1. This approach of quaternary structural alignment considerably negates the effect of crystallographic artefacts. However, conformational changes at the residue level could not be considered (Figure 2.5).

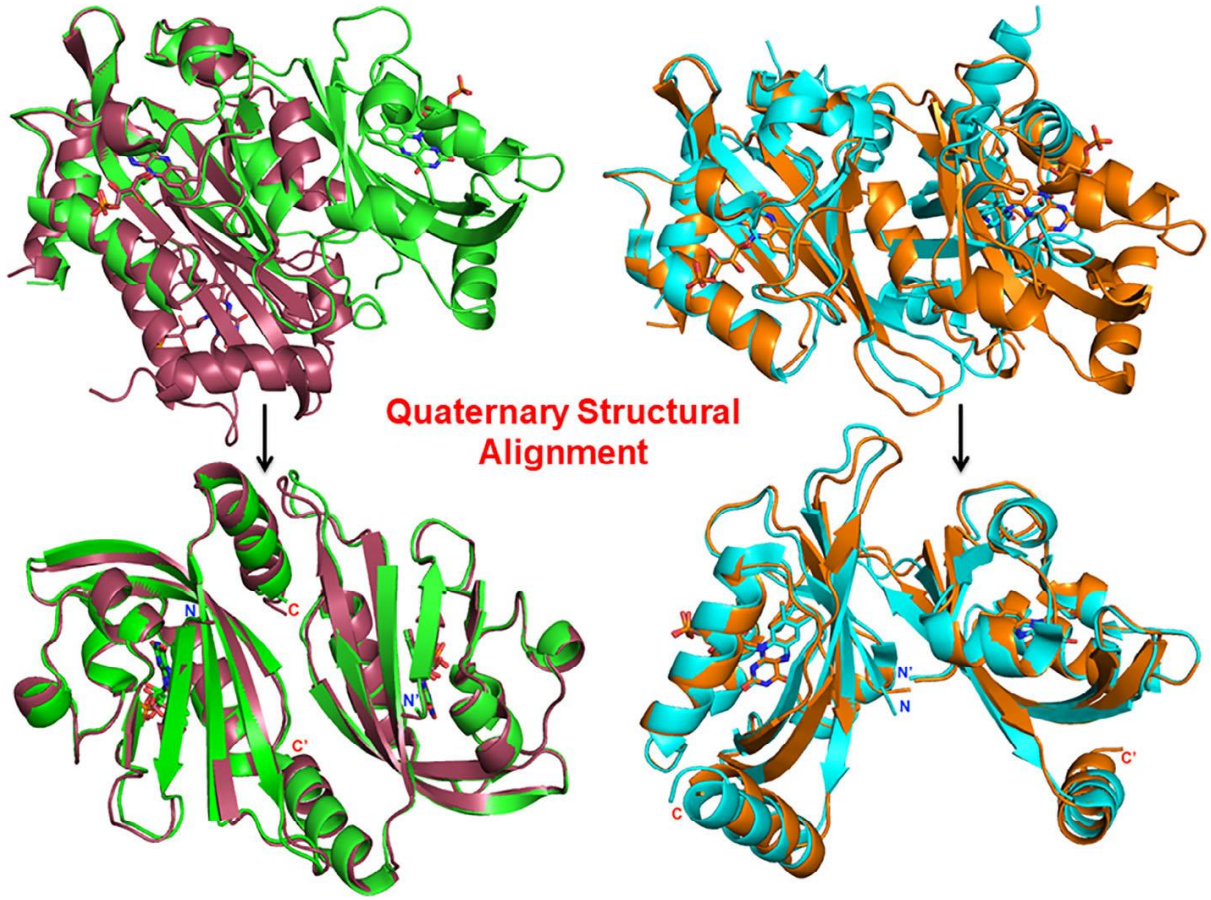

Figure 2.5: Quaternary structural alignment of *Vf*Aureo1 with *Pt*Aureo1 to achieve biologically meaningful parallel dimer. The dark-state structure of *Vf*Aureo1 3UE6 (in green colour) is aligned to 5A8B (in salmon colour) and lit-state structure of *Vf*Aureo1 3ULF (in orange) is aligned to 5DKL (in cyan colour) by rotation and translation of monomeric units of *Vf*Aureo1.

Revised RIG/DN analysis on altered VfAureo1 LOV structure reveals that (Gln258, Asn286) and (Lys269, Val282) in light differential network (LDN) and (Ile274, Ile270) in DDN are most important interactions. Not only the exact same results were predicted in earlier network study, this result is in full agreement with our experimental results (Table 3, Figure 2.3) as well. Interestingly, edges between Val309-Val314, Pro204-Leu212, found insignificant in experiments did not show up either in the revised network analysis (Figure 2.6). Moreover Gln332-Cys283 interaction, also found to be of very less significance in our experiment, did not appear in revised DN analysis (Figure 2.6).

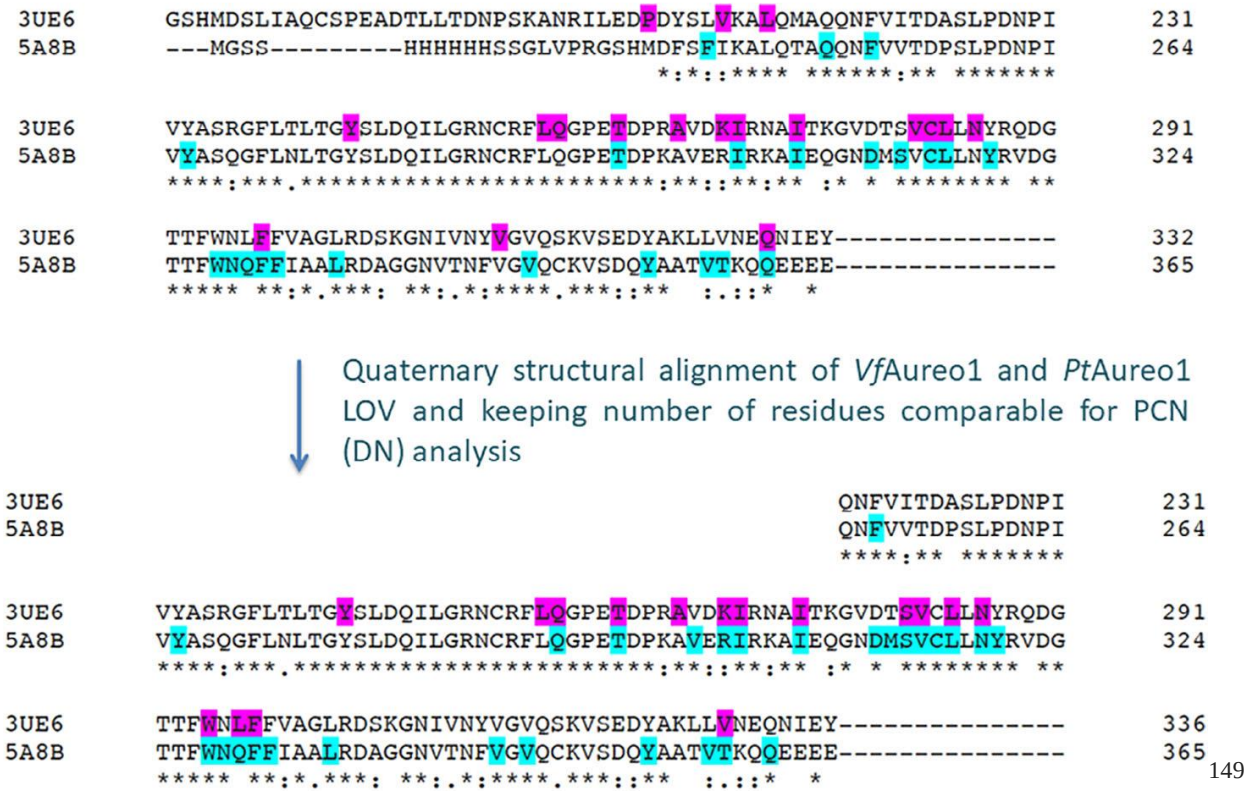

Figure 2.6: Distribution of residue found to be interacting uniquely, either in dark- or light-state differential network (DDN/LDN) in *Vaucheria frigida* aureochrome1 (*Vf*Aureo1) and *Phaeodactylum tricornutum* aureochrome (*Pt*Aureo1) light-oxygen-voltage (LOV), aligned pairwise. Quaternary structural alignment not only improves results from network analyses but also significantly corroborates experimental findings. Residues unique to *Vf*Aureo1 LOV (3UE6) are highlighted in pink, whereas residues unique to *Pt*Aureo1 LOV (5A8B) are in cyan.

In this objective, we attempted to address the importance of allosterically coupled amino acid residues, and effect of edge deletion on residue interaction network. Although complete edge deletion is a myth in real scenario, effort was taken to minimize the interaction to lowest possible magnitude, which, showed consistent agreement with RIG. Notion of quaternary structural alignment was introduced as an alternative

to extract biologically meaningful information from crystal structures.

4.3 Objective 3: The third and final objective is structure-guided design of optogenetic scaffold from Aureochromes. Given widespread use of *As*LOV2 in LOV-based optogenetics tools we considered using the same as a substitution to *To*AuL, to design synthetic photoreceptor-transcription factor. *As*LOV2 has been conveniently used in several synthetic proteins taking advantage of the C-terminal effector both in natural and synthetic constructs. However, several DNA-binding effector domains are located at the N-terminus to the sensor. Examples include bZIP in Aureochromes or bHLH in ARNT/HIF-1α etc. Therefore, using a sensor which is mostly successful in combination with a C-terminal effector has been a challenge in our design strategy. However, instead of Jα unfolding, we capitalized on the unfolding of A`α in *As*LOV2 and fused this sensor with bZIP of *To*Aureo1 according to the following orientation (Figure 3.1).

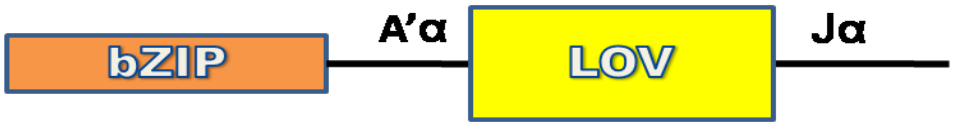

>*As*_LOV

MLATTLERIEKNFVITDPRLPDNPIIFASDSFLQLTEYSREEILGRNCRFLQGPETDRATVRKIRDAIDNQTEVTVQL
INYTKSGKKFWNLFHLQPMRDQKGDVQYFIGVQLDGTEHVRDAAEREGVMLIKKTAENI

>To_bZIP

RRERNREHAKRSRIRKKFLLESLQQSVSLLKEENGKLKNAIRTHLGEKE

Figure3.1: Orientation and sequence of *AsTo*bZ (*Thalassiosira oceanica* bZIP domain and *Avena sativa*Phot1 LOV2).

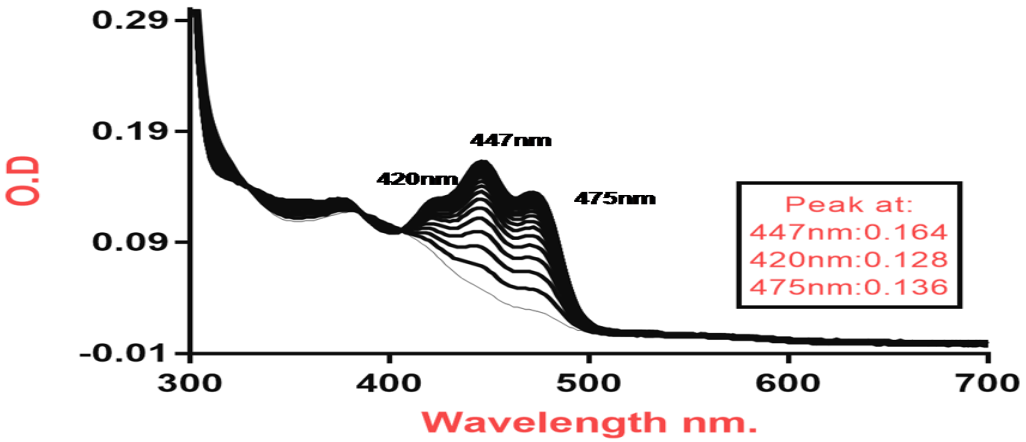

Figure 3.2: Graph for dark recovery kinetics of *AsTo*bZ.

The chimeric construct thus generated is named *AsTo*bZ. *AsTo*bZ could be expressed well and purified to sufficient homogeneity. Kinetics conducted by UV-Vis spectroscopy reveals that the light-state lifetime of *AsTo*bZ is slightly reduced (69 seconds) in comparison to 80 seconds in native *As*LOV2. However, the rate constant *K* (1.017 $x10^{-2}$ $s^{-1)}$, is in same order of magnitude as that of WT ($1.2x10^{-2}$) with a standard error of 0.4 $x10^{-6}$ s^{-1} [51,73](Fig:3.2). Thus we were able to generate a fusion construct which has considerably faster dark-state recovery rate than original *To*AubZL. Generation of such light controlled transcription factors could facilitate a next layer of control in several biological pathways.

After collecting purified protein it was subjected to CD spectroscopy for secondary structure analysis. Data analysis of *AsTo*bZ was done using BeStSel[156] method which have been derived from DSSP[157].

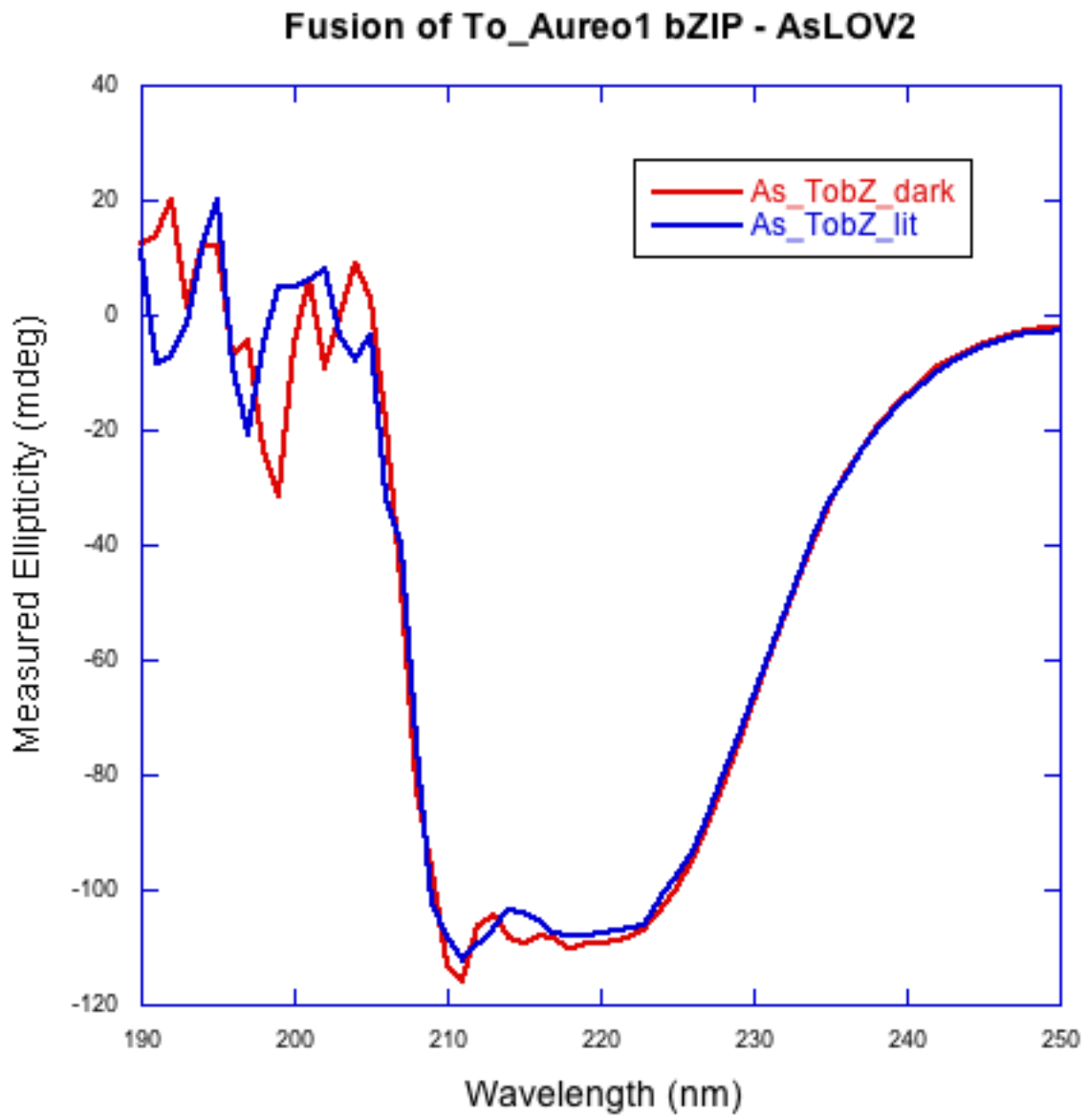

Fig 3.3: CD spectra for *AsTo*bZ in dark and lit state

Secondary structures (%)	**Dark** (**RMSD: 0.1454)**	**Lit** **(RMSD: 0.1445)**
Helix 1(regular helix)	0.6	0.6
Helix 2 (distorted helix)	0.0	0.2
Anti 1 (left hand twisted anti-parallel β sheet)	5.1	5.3
Anti 2 (slight right hand twisted anti-parallel β sheet)	19.4	19.0

Anti 3 (Right hand twisted anti-parallelβ sheet)	21.3	20.3
Parallel β sheet	0.0	0.0
Turn	13.3	13.5
Others (3.10 helix, л helix, β bridge, bend, loop, irregular and invisible region of the the structure)	40.3	40.9

Table 3.4: Percentage of secondary structures in *AsTo*bZ (dark and lit state) by *BeStSel* method.

CD measurements and *BeStSe*l analysis of *AsTo*bZ shows that lit state structure consists of distorted helix unlike the dark structure. This is possibly due to unfolding of Ja or A`a, which is common in *As*LOV2 (Fig: 3.3). Changes in the anti-parallel β content are minimal, considering very conservative nature LOV core. There is also increase in turn and other higher order structures, on photon absorption.

EMSA with *AsTo*bZ was performed using the following oligo :

EMSA_bZIP_FP2: 5′TGT CCT TGG CTG ACG TCA GCC AAG CAC 3′

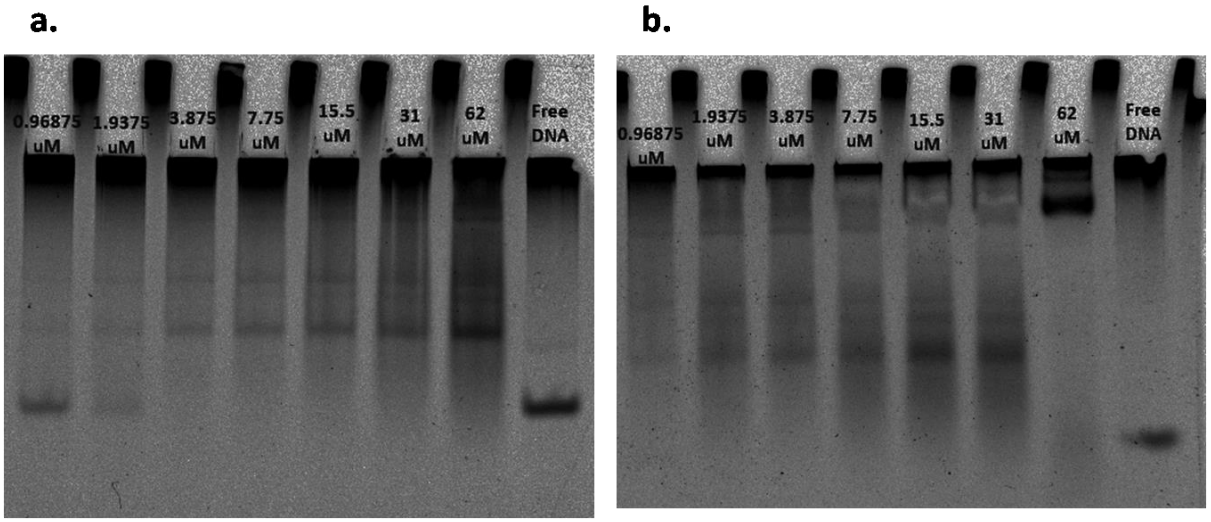

Figure 3.5:a. EMSA of *AsTo*bZ in dark condition b. EMSA of *AsTo*bZ in presence of light.

The figure shows free DNA i.e. binding to no binding in dark condition while complete binding is observed in presence of light for same concentration of protein and DNA. Preliminary EMSA studies show light regulated DNA binding as well as higher order structure formation. However, this needs to be validated by further experimentation.

5. CONCLUSION:

With an effective combination of theory and experiments, we have characterized BL-responsive LOV photoreceptors, especially *Vf*Aureo1 and *To*Aureo1. Structural and functional characterization is not only important to unravel mechanistic insights of LOV signaling but also extremely important to explain natural phenomena as well as optogenetic designs. Except heterogeneous linkers, *Vf*Aureo1 and *To*Aureo1 show high sequence/structure conservation in bZIP and LOV domains. However, subtle changes in few amino acid positions make *To*Aureo1 LOV a slow-cycling variant in comparison to *Vf*Aureo1 LOV. Our dual approach of network-driven-experiments and experiments-driven-network studies have helped identify residue interactions, suitable to generate temporal scaffolds for optogenetics. Further the notion of quaternary structural alignment was introduced to address a rather fundamental problem--reflection of crystallographic artifacts in RIG. Comparable dark reversal kinetics of *To*Aureo1 LOV as well as *To*AubZL construct confirmed domain modularity--one of the important criteria for optogenetic design. Taking advantage of its modularity a synthetic LOV-photoreceptor *AsTo*bZ was generated which showed faster dark reversal kinetics. Recent evidences show, altered photocycle of Phototropin 1 and 2 in *Arabidopsis thaliana* resulted in increased biomass[158]. In the long term objective, aureochrome based optogenetics could be used in enhanced production of algal biomass. To conclude, this study is a stepping stone towards understanding several BL-responsive photoreceptors especially aureochromes and its application in optogenetics. In the near future we look forward to use optogenetics as an alternative to chemical remedy: both in medicine and agriculture.

APPENDIX

Primers required for experiments arranged according to the objectives:

Objective 1: ***Thalassiosira oceanica***

ToAuL FP: 5'- GGT CGC TAG CAT GCA GGC GCT GGC GG -3'

ToAubZL

FP: 5'- GATCGGATCCATGAGCAACGCGGGC -3'

RP: 5'- GTA CCC TAG GTT ACG CAT CCG CTT CAT C -3'

ToAubZL_hs-ka_

FP_V1-5`CGC AAC CGC GAA AGC GCG GCA CGC AGC CGC ATT C 3`

RP_V1-5`GAA TGC GGC TGC GTG CCG CGC TTT CGC GGT TGC G 3`

ToAubZL_hs-kl_

FP_V2-5'CGC AAC CGC GAA AGC GCG CTA CGC AGC CGC ATT C 3`

RP_V2-5`GAA TGC GGC TGC GTA GCG CGC TTT CGC GGT TGC G 3'

Objective 2: Vaucheria frigida

AuLOV_FP1: 5'- CTA GGC TAG CGA TTC ACT TAT TGC TCA ATG TTC -3'

AL_RP4: 5'- AGC TGA GCT CTC ATT TAT ATT CAA TAT TTT GTT CAT TAA C -3'

F298A:

FP: 5'-CAT TCT GGA ATC TTG CCT TCG TTG CTG GAC-3'

RP:5'-GTC CAG CAA CGA AGG CAA GAT TCC AGA ATG-3'

L284A:

FP: 5'-GTT GAT ACA TCA GTT TGT GCT CTT AAT TAT AGA CAA GAT GG-3'

RP: 5'-CCA TCT TGT CTA TAA TTA AGA GCA CAA ACT GAT GTA TCA AC-3'

Q258A:

FP: 5'-TGT AGA TTC CTT GCA GGA CCA GAA ACA G-3'

RP: 5'-CTG TTT CTG GTC CTG CAA GGA ATC TAC A-3'

N286A:

FP: 5'-CAG TTT GTC TTC TTG CTT ATA GAC AAG ATG GAA C-3'

RP: 5'-GTT CCA TCT TGT CTA TAA GCA AGA AGA CAA ACT G-3'

A266E:

FP: 5'-GAA ACA GAT CCA AGA GAA GTT GAT AAA ATT AG-3'

RP: 5'-CTA ATT TTA TCA ACT TCT CTT GGA TCT GTT TC-3'

Y244F:

FP: 5'-TCC TTA CAC TTA CAG GAT TTT CAC TTG AT-3'

RP: 5'-GAA TTT GAT CAA GTG AAA ATC CTG TAA GT-3'

L257I:

FP: 5'-GAA ATT GTA GAT TCA TTC AAG GAC CAG AAA CAG-3'

RP: 5'-CTG TTT CTG GTC CTT GAA TGA ATC TAC AAT TTC-3'

K269N:

FP: 5'-CCA AGA GCT GTT GAT AAC ATT AGA AAT GG-3'

RP:5'-GTA ATA GCA TTT CTA ATG TTA TCA ACA GC-3'

V282A:

FP: 5'-GGA GTT GAT ACA TCA GCT TGT CTT CTT AAT TAT AG-3'

RP: 5'-CTA TAA TTA AGA CAA GCT GAT GTA TCA ACT CC-3'

T262A:

FP: 5'-CAA GGA CCA GAA GCA GAT CCA AGA GCT G-3'

RP: 5'-CAG CTC TTG GAT CTG CTT CTG GTC CTT G-3'

V209A:

FP: 5'-CAG ATT ATT CAC TTG CTA AAG CTC TTC AAA TG-3'

RP: 5'-CAT TTG AGG AGC TTT AGC AAG TGA ATA ATC TG-3'

V314A:

FP: 5'-GAA ATA TTG TTA ATT ATG CTG GAG TTC AAT CAA AAG-3'

RP: 5'-CTT TTG ATT GAA CTC CAG CAT AAT TAA CAA TAT TTC-3'

P204A:

FP: 5'-AAT AGA ATT CTT GAA GATGCA GAT TAT TCA CTT GTT AAA G-3'

RP: 5'-CTT TAA CAA GTG AAT AAT CTG CAT CTT CAA GAA TTC TAT T-3'

L212P:

FP: 5'-CAC TGT TTA AAG CTC CTC AAA TGG CTC AAC-3'

RP: 5'-GTT GAG CCA TTT GAG GAG CTT TAA CAA GTG-3'

C283A:

FP: 5'-GTT GAT ACA TCA GTT GCT CTT CTT AAT TAT AG-3'

RP: 5'-CTA TAA TTA AGA AGA GCA ACT GAT GTA TCA AC-3'

Q332A:

FP: 5'-CTT CTT GTT AAT GAA GCA AAT ATT GAA TAT AAA G-3'

RP: 5'-CTT TAT ATT CAA TAT TTG CTT CAT TAA CAA GAA G-3'

I270M:

FP: 5'-CCA AGA GCT GTT GAT AAA ATG AGA AAT-3'

RP: 5'-GTA ATA GCA TTT CTC ATT TTA TCA ACA-3'

I274V:

FP: 5'-GAT AAA ATT AGA AAT GCT GTT ACA AAA GG-3'

RP: 5'-GAT GTA TCA ACT CCT TTTGTA ACA GCA TT-3'

Objective 3: Thallasiosira oceanica(bZIP) + Avena sativa (LOV)

Forward primer of bZip:

5'- GAT CGC TAG CAT GCG CCG CGA ACG CAA C -3'

Reverse primer fusion overhang:

5'- GGT GGT CGC CAG CAT TTC TTT TTC GCC CAG -3'

Forward primer of oat LOV fusion overhang:

5'- CTG GGC GAA AAA GAA ATG CTG GCG ACC ACC -3'

Reverse primer of oat LOV:

5'- GAT CGA GCT CTT ACA GTT CTT TCG CCG CTT C -3'

Abbreviations:

Thallassioira oceanica Aurechrome (bZIP+LOV): *To*AubZL; (LOV): *To*AuL

Vaucheria frigida Aureochrome: *Vf*Au

Avena sativa (LOV) + *Thallassiosira oceanica* (bZIP): *AsTo*bZ

Residue interaction Graph: RIG ; Residue Interaction Network: RIN

Dark Differential Network: DDN; Light Differential Network: LDN

Blue Light: BL

Wild Type: WT

References:

1. van der Horst MA, Hellingwerf KJ. Photoreceptor Proteins, "Star Actors of Modern Times": A Review of the Functional Dynamics in the Structure of Representative Members of Six Different Photoreceptor Families. *Acc Chem Res*. 2004;37(1):13-20. doi:10.1021/ar020219d

2. Christie JM, Gawthorne J, Young G, Fraser NJ, Roe AJ. LOV to BLUF: Flavoprotein contributions to the optogenetic toolkit. *Mol Plant*. 2012;5(3):533-544. doi:10.1093/mp/sss020

3. Rockwell NC, Lagarias JC. A Brief History of Phytochromes. *ChemPhysChem*. 2010;11(6):1172-1180. doi:10.1002/cphc.200900894

4. Chaves I, Pokorny R, Byrdin M, et al. The cryptochromes: blue light photoreceptors in plants and animals. *Annu Rev Plant Biol*. 2011;62:335-364. doi:10.1146/annurev-arplant-042110-103759

5. Banerjee S, Mitra D. Structural Basis of Design and Engineering for Advanced Plant Optogenetics. *Trends Plant Sci*. 2020;25(1):35-65. doi:10.1016/j.tplants.2019.10.002

6. Losi A, Gardner KH, Möglich A. Blue-Light Receptors for Optogenetics. *Chem Rev*. 2018;118(21):10659-10709. doi:10.1021/acs.chemrev.8b00163

7. Losi A, Gärtner W. The Evolution of Flavin-Binding Photoreceptors: An Ancient Chromophore Serving Trendy Blue-Light Sensors. *Annu Rev Plant Biol*. 2012;63(1):49-72. doi:10.1146/annurev-arplant-042811-105538

8. Huala E. Arabidopsis NPH1: A Protein Kinase with a Putative Redox-Sensing Domain. *Science (80-)*. 1997;278(5346):2120-2123. doi:10.1126/science.278.5346.2120

9. Losi A, Gärtner W. Shedding (blue) light on algal gene expression. *Proc Natl Acad Sci U S A*. 2008;105(1):7-8. doi:10.1073/pnas.0710523105

10. Kirk JTO. *Light and Photosynthesis in Aquatic Ecosystems*. Cambridge University Press; 2010. doi:10.1017/CBO9781139168212

11. Depauw FA, Rogato A, Ribera d'Alcala M, Falciatore A. Exploring the molecular basis of responses to light in marine diatoms. *J Exp Bot*. 2012;63(4):1575-1591. doi:10.1093/jxb/ers005

12. Christie JM, Blackwood L, Petersen J, Sullivan S. Plant Flavoprotein Photoreceptors. *Plant Cell Physiol*. 2015;56(3):401-413. doi:10.1093/pcp/pcu196

13. Suetsugu N, Wada M. Evolution of Three LOV Blue Light Receptor Families in Green Plants and Photosynthetic Stramenopiles: Phototropin, ZTL/FKF1/LKP2 and Aureochrome. *Plant Cell Physiol*. 2013;54(1):8-23. doi:10.1093/pcp/pcs165

14. Holzer W, Penzkofer A, Hegemann P. Photopysical and photochemical excitation and relaxation dynamics of LOV domains of phot from Chlamydomonas reinhardtii. *J Lumin*. 2005;112(1-4):444-448. doi:10.1016/j.jlumin.2004.09.069

15. Salomon M, Christie JM, Knieb E, Lempert U, Briggs WR. Photochemical and mutational analysis of the FMN-binding domains of the plant blue light receptor, phototropin. *Biochemistry*. 2000;39(31):9401-9410. doi:10.1021/bi000585+

16. Kottke T, Heberle J, Hehn D, Dick B, Hegemann P. Phot-LOV1: Photocycle of a Blue-Light Receptor Domain from the Green Alga Chlamydomonas reinhardtii. *Biophys J*. 2003;84(2):1192-1201. doi:10.1016/S0006-3495(03)74933-9

17. Baier J, Maisch T, Maier M, Engel E, Landthaler M, Bäumler W. Singlet Oxygen Generation by UVA Light Exposure of Endogenous Photosensitizers. *Biophys J*. 2006;91(4):1452-1459. doi:10.1529/biophysj.106.082388

18. Drepper T, Gensch T, Pohl M. Advanced in vivo applications of blue light photoreceptors as alternative fluorescent

proteins. *Photochem Photobiol Sci*. 2013;12(7):1125-1134. doi:10.1039/c3pp50040c

19. Losi A, Gärtner W. Old chromophores, new photoactivation paradigms, trendy applications: Flavins in blue light-sensing photoreceptors. *Photochem Photobiol*. 2011;87(3):491-510. doi:10.1111/j.1751-1097.2011.00913.x

20. Banerjee A, Herman E, Serif M, et al. Allosteric communication between DNA-binding and light-responsive domains of diatom class I aureochromes. *Nucleic Acids Res*. 2016;44(12):5957-5970. doi:10.1093/nar/gkw420

21. Cock JM, Sterck L, Rouzé P, et al. The Ectocarpus genome and the independent evolution of multicellularity in brown algae. *Nature*. 2010;465(7298):617-621. doi:10.1038/nature09016

22. Swartz TE, Corchnoy SB, Christie JM, et al. The Photocycle of a Flavin-binding Domain of the Blue Light Photoreceptor Phototropin. *J Biol Chem*. 2001;276(39):36493-36500. doi:10.1074/jbc.M103114200

23. Purcell EB, McDonald CA, Palfey BA, Crosson S. An Analysis of the Solution Structure and Signaling Mechanism of LovK, a Sensor Histidine Kinase Integrating Light and Redox Signals. *Biochemistry*. 2010;49(31):6761-6770. doi:10.1021/bi1006404

24. Arents JC, Perez MA, Hendriks J, Hellingwerf KJ. On the midpoint potential of the FAD chromophore in a BLUF-domain containing photoreceptor protein. *FEBS Lett*. 2011;585(1):167-172. doi:10.1016/j.febslet.2010.11.035

25. Jurk M, Schramm P, Schmieder P. The blue-light receptor YtvA from Bacillus subtilis is permanently incorporated into the stressosome independent of the illumination state. *Biochem Biophys Res Commun*. 2013;432(3):499-503. doi:10.1016/j.bbrc.2013.02.025

26. Marles-Wright J, Lewis RJ. The Bacillus subtilis stressosome. *Commun Integr Biol*. 2008;1(2):182-184. doi:10.4161/cib.1.2.7225

27. Capra EJ, Laub MT. Evolution of Two-Component Signal Transduction Systems. *Annu Rev Microbiol*. 2012;66(1):325-347. doi:10.1146/annurev-micro-092611-150039

28. Bowler C, Allen AE, Badger JH, et al. The Phaeodactylum genome reveals the evolutionary history of diatom genomes. *Nature*. 2008;456(7219):239-244. doi:10.1038/nature07410

29. Armbrust E V. The Genome of the Diatom Thalassiosira Pseudonana: Ecology, Evolution, and Metabolism. *Science (80-)*. 2004;306(5693):79-86. doi:10.1126/science.1101156

30. Takahashi F, Yamagata D, Ishikawa M, et al. AUREOCHROME, a photoreceptor required for photomorphogenesis in stramenopiles. *Proc Natl Acad Sci*. 2007;104(49):19625-19630. doi:10.1073/pnas.0707692104

31. Ishikawa M, Takahashi F, Nozaki H, Nagasato C, Motomura T, Kataoka H. Distribution and phylogeny of the blue light receptors aureochromes in eukaryotes. *Planta*. 2009;230(3):543-552. doi:10.1007/s00425-009-0967-6

32. Takahashi F, Hishinuma T, Kataoka H. Blue Light-Induced Branching in Vaucheria. Requirement of Nuclear Accumulation in the Irradiated Region. *Plant Cell Physiol*. 2001;42(3):274-285. doi:10.1093/pcp/pce033

33. Harper SM, Christie JM, Gardner KH. Disruption of the LOV-J?? helix interaction activates phototropin kinase activity. *Biochemistry*. 2004;43(51):16184-16192. doi:10.1021/bi048092i

34. Christie JM. Phototropin Blue-Light Receptors. *Annu Rev Plant Biol*. 2007;58(1):21-45. doi:10.1146/annurev.arplant.58.032806.103951

35. Lommer M. Acclimation and adaptation to low-iron conditions in the marine diatoms Phaeodactylum tricornutum and Thalassiosira oceanica. Published online 2012.

36. Armbrust EV. The life of diatoms in the world's oceans. *Nature*. 2009;459(7244):185-192. doi:10.1038/nature08057

37. Martin JH, Coale KH, Johnson KS, et al. Testing the iron hypothesis in ecosystems of the equatorial Pacific Ocean. *Nature*. 1994;371(6493):123-129. doi:10.1038/371123a0

38. Haan H. Effects of metal speciation on growth of phytoplankton with special reference to iron. *Hydrobiol Bull*. 1984;18(2):85-94. doi:10.1007/BF02257047

39. Kianianmomeni A, Hallmann A. Algal photoreceptors: in vivo functions and potential applications. *Planta*. 2014;239(1):1-26. doi:10.1007/s00425-013-1962-5

40. Radakovits R, Jinkerson RE, Fuerstenberg SI, et al. Draft genome sequence and genetic transformation of the oleaginous alga Nannochloropsis gaditana. *Nat Commun*. 2012;3(1):686. doi:10.1038/ncomms1688

41. Huysman MJ, Martens C, Vandepoele K, et al. Genome-wide analysis of the diatom cell cycle unveils a novel type of cyclins involved in environmental signaling. *Genome Biol*. 2010;11(2):R17. doi:10.1186/gb-2010-11-2-r17

42. Schellenberger Costa B, Sachse M, Jungandreas A, et al. Aureochrome 1a Is Involved in the Photoacclimation of the Diatom Phaeodactylum tricornutum. *PLoS One*. 2013;8(9). doi:10.1371/journal.pone.0074451

43. Huysman MJJ, Fortunato AE, Matthijs M, et al. AUREOCHROME1a-Mediated Induction of the Diatom-Specific Cyclin dsCYC2 Controls the Onset of Cell Division in Diatoms (Phaeodactylum tricornutum). *Plant Cell*. 2013;25(1):215-228. doi:10.1105/tpc.112.106377

44. Herman E, Sachse M, Kroth PG, Kottke T. Blue-Light-Induced Unfolding of the Jα Helix Allows for the Dimerization of Aureochrome-LOV from the Diatom Phaeodactylum tricornutum. *Biochemistry*. 2013;52(18):3094-3101. doi:10.1021/bi400197u

45. Herman E, Kottke T. Allosterically Regulated Unfolding of the A′α Helix Exposes the Dimerization Site of the Blue-Light-Sensing Aureochrome-LOV Domain. *Biochemistry*. 2015;54(7):1484-1492. doi:10.1021/bi501509z

46. Matiiv AB, Chekunova EM. Aureochromes – Blue Light Receptors. *Biochem*. 2018;83(6):662-673. doi:10.1134/S0006297918060044

47. Gekakis N. Role of the CLOCK Protein in the Mammalian Circadian Mechanism. *Science (80-)*. 1998;280(5369):1564-1569. doi:10.1126/science.280.5369.1564

48. Hill S, Austin S, Eydmann T, Jones T, Dixon R. Azotobacter vinelandii NIFL is a flavoprotein that modulates transcriptional activation of nitrogen-fixation genes via a redox-sensitive switch. *Proc Natl Acad Sci*. 1996;93(5):2143-2148. doi:10.1073/pnas.93.5.2143

49. Hiraoka M, Nakajima T, Furukawa T. Mechanisms of Functional Disturbances of Various HERG Mutations in Patients with Long QT Syndrome 2 (LQT2). In: ; 2003:399-408. doi:10.1007/978-1-4615-0355-2_28

50. Jakoby M, Weisshaar B, Dröge-Laser W, et al. bZIP transcription factors in Arabidopsis. *Trends Plant Sci*. 2002;7(3):106-111. doi:10.1016/S1360-1385(01)02223-3

51. Mitra D, Yang X, Moffat K. Crystal structures of aureochrome1 LOV suggest new design strategies for optogenetics. *Structure*. 2012;20(4):698-706. doi:10.1016/j.str.2012.02.016

52. Ellenberger TE, Brandl CJ, Struhl K, Harrison SC. The GCN4 basic region leucine zipper binds DNA as a dimer of uninterrupted α Helices: Crystal structure of the protein-DNA complex. *Cell*. 1992;71(7):1223-1237. doi:10.1016/S0092-8674(05)80070-4

53. Vinson C, Acharya A, Taparowsky EJ. Deciphering B-ZIP transcription factor interactions in vitro and in vivo. *Biochim Biophys Acta - Gene Struct Expr*. 2006;1759(1-2):4-12. doi:10.1016/j.bbaexp.2005.12.005

54. Hisatomi O, Takeuchi K, Zikihara K, et al. Blue Light-Induced Conformational Changes in a Light-Regulated Transcription Factor, Aureochrome-1. *Plant Cell Physiol*. 2013;54(1):93-106. doi:10.1093/pcp/pcs160

55. Toyooka T, Hisatomi O, Takahashi F, Kataoka H, Terazima M. Photoreactions of Aureochrome-1. *Biophys J*. 2011;100(11):2801-2809. doi:10.1016/j.bpj.2011.02.043

56. Barth A, Georg H, Kreutz W, Mäntele W. Changes of molecular structure and interaction in the catalytic cycle of sarcoplasmic reticulum Ca2+- ATPase. In: *The Sodium Pump*. Steinkopff; 1994:135-138. doi:10.1007/978-3-642-72511-1_24

57. Kerruth S, Ataka K, Frey D, Schlichting I, Heberle J. Aureochrome 1 Illuminated: Structural Changes of a Transcription Factor Probed by Molecular Spectroscopy. Sauer M, ed. *PLoS One*. 2014;9(7):e103307. doi:10.1371/journal.pone.0103307

58. Henry JT, Crosson S. Ligand-Binding PAS Domains in a Genomic, Cellular, and Structural Context. *Annu Rev Microbiol*. 2011;65(1):261-286. doi:10.1146/annurev-micro-121809-151631

59. Pellequer J-L, Wager-Smith KA, Kay SA, Getzoff ED. Photoactive yellow protein: A structural prototype for the three-dimensional fold of the PAS domain superfamily. *Proc Natl Acad Sci*. 1998;95(11):5884-5890. doi:10.1073/pnas.95.11.5884

60. Ponting CP, Aravind L. PAS: a multifunctional domain family comes to light. *Curr Biol*. 1997;7(11):R674-R677. doi:10.1016/S0960-9822(06)00352-6

61. Taylor BL, Zhulin IB. PAS domains: internal sensors of oxygen, redox potential, and light. *Microbiol Mol Biol Rev*.

1999;63(2):479-506. doi:1092-2172/99

62. Borgstahl GEO, Williams DR, Getzoff ED. 1.4 .ANG. Structure of Photoactive Yellow Protein, a Cytosolic Photoreceptor: Unusual Fold, Active Site, and Chromophore. *Biochemistry*. 1995;34(19):6278-6287. doi:10.1021/bi00019a004

63. Sean Crosson and Keith Moffat. No Title. *PNAS*. 2001;98(051520298):6.

64. Miyatake H, Mukai M, Park S-Y, et al. Sensory mechanism of oxygen sensor FixL from Rhizobium meliloti : crystallographic, mutagenesis and resonance raman spectroscopic studies 1 1Edited by K. Nagai. *J Mol Biol*. 2000;301(2):415-431. doi:10.1006/jmbi.2000.3954

65. Möglich A, Ayers R a., Moffat K. Design and Signaling Mechanism of Light-Regulated Histidine Kinases. *J Mol Biol*. 2009;385(5):1433-1444. doi:10.1016/j.jmb.2008.12.017

66. Gu J-D, Mitchell R. Biodeterioration. In: *The Prokaryotes*. Springer Berlin Heidelberg; 2013:309-341. doi:10.1007/978-3-642-31331-8_31

67. Adaixo R, Harley C a., Castro-Rodrigues AF, Morais-Cabral JH. Structural Properties of PAS Domains from the KCNH Potassium Channels. *PLoS One*. 2013;8(3). doi:10.1371/journal.pone.0059265

68. Möglich A, Ayers R a., Moffat K. Structure and Signaling Mechanism of Per-ARNT-Sim Domains. *Structure*. 2009;17(10):1282-1294. doi:10.1016/j.str.2009.08.011

69. Hoff WD, Dux P, Hard K, et al. Thiol ester-linked p-coumaric acid as a new photoactive prosthetic group in a protein with rhodopsin-like photochemistry. *Biochemistry*. 1994;33(47):13959-13962. doi:10.1021/bi00251a001

70. Zoltowski BD, Schwerdtfeger C, Widom J, et al. Conformational Switching in the Fungal Light Sensor Vivid. *Science (80-)*. 2007;316(5827):1054-1057. doi:10.1126/science.1137128

71. Alexandre MTA, Domratcheva T, Bonetti C, et al. Primary Reactions of the LOV2 Domain of Phototropin Studied with Ultrafast Mid-Infrared Spectroscopy and Quantum Chemistry. *Biophys J*. 2009;97(1):227-237. doi:10.1016/j.bpj.2009.01.066

72. Halavaty AS, Moffat K. N- and C-Terminal Flanking Regions Modulate Light-Induced Signal Transduction in the LOV2 Domain of the Blue Light Sensor Phototropin 1 from Avena sativa † , ‡. *Biochemistry*. 2007;46(49):14001-14009. doi:10.1021/bi701543e

73. Zayner JP, Antoniou C, Sosnick TR. The Amino-Terminal Helix Modulates Light-Activated Conformational Changes in AsLOV2. *J Mol Biol*. 2012;419(1-2):61-74. doi:10.1016/j.jmb.2012.02.037

74. Leong Y, Ker P, Jamaludin M, et al. UV-Vis Spectroscopy: A New Approach for Assessing the Color Index of Transformer Insulating Oil. *Sensors*. 2018;18(7):2175. doi:10.3390/s18072175

75. Röllen K, Granzin J, Batra-Safferling R, Stadler AM. Small-angle X-ray scattering study of the kinetics of light-dark transition in a LOV protein. Kursula P, ed. *PLoS One*. 2018;13(7):e0200746. doi:10.1371/journal.pone.0200746

76. Lin Y-C, Fu H-Y, Yang C-S. Phototaxis of Haloarcula marismortui Revealed Through a Novel Microbial Motion Analysis Algorithm. *Photochem Photobiol*. 2010;86(5):1084-1090. doi:10.1111/j.1751-1097.2010.00768.x

77. Vaidya AT, Chen C-H, Dunlap JC, Loros JJ, Crane BR. Structure of a Light-Activated LOV Protein Dimer That Regulates Transcription. *Sci Signal*. 2011;4(184):ra50-ra50. doi:10.1126/scisignal.2001945

78. Chen C-H, DeMay BS, Gladfelter AS, Dunlap JC, Loros JJ. Physical interaction between VIVID and white collar complex regulates photoadaptation in Neurospora. *Proc Natl Acad Sci*. 2010;107(38):16715-16720. doi:10.1073/pnas.1011190107

79. Aihara Y, Yamamoto T, Okajima K, et al. Mutations in N-terminal Flanking Region of Blue Light-sensing Light-Oxygen and Voltage 2 (LOV2) Domain Disrupt Its Repressive Activity on Kinase Domain in the Chlamydomonas Phototropin. *J Biol Chem*. 2012;287(13):9901-9909. doi:10.1074/jbc.M111.324723

80. Okajima K, Kashojiya S, Tokutomi S. Photosensitivity of Kinase Activation by Blue Light Involves the Lifetime of a Cysteinyl-Flavin Adduct Intermediate, S390, in the Photoreaction Cycle of the LOV2 Domain in Phototropin, a Plant Blue Light Receptor. *J Biol Chem*. 2012;287(49):40972-40981. doi:10.1074/jbc.M112.406512

81. Bittl R, Kay CWM, Weber S, Hegemann P. Characterization of a Flavin Radical Product in a C57M Mutant of a LOV1 Domain by Electron Paramagnetic Resonance †. *Biochemistry*. 2003;42(28):8506-8512. doi:10.1021/bi034123i

82. Kay CWM, Schleicher E, Kuppig A, et al. Blue Light Perception in Plants. *J Biol Chem*. 2003;278(13):10973-10982. doi:10.1074/jbc.M205509200

83. Richter G, Weber S, Römisch W, Bacher A, Fischer M, Eisenreich W. Photochemically Induced Dynamic Nuclear Polarization in a C450A Mutant of the LOV2 Domain of the Avena s ativa Blue-Light Receptor Phototropin. *J Am Chem Soc*. 2005;127(49):17245-17252. doi:10.1021/ja053785n

84. Lanzl K, Sanden-Flohe M v., Kutta R-J, Dick B. Photoreaction of mutated LOV photoreceptor domains from Chlamydomonas reinhardtii with aliphatic mercaptans: implications for the mechanism of wild type LOV. *Phys Chem Chem Phys*. 2010;12(25):6594. doi:10.1039/b922408d

85. Zoltowski BD, Gardner KH. Tripping the light fantastic: Blue-light photoreceptors as examples of environmentally modulated protein-protein interactions. *Biochemistry*. 2011;50(1):4-16. doi:10.1021/bi101665s

86. Lokhandwala J, Hopkins HC, Rodriguez-Iglesias A, Dattenböck C, Schmoll M, Zoltowski BD. Structural Biochemistry of a Fungal LOV Domain Photoreceptor Reveals an Evolutionarily Conserved Pathway Integrating Light and Oxidative Stress. *Structure*. 2015;23(1):116-125. doi:10.1016/j.str.2014.10.020

87. Conrad KS, Manahan CC, Crane BR. Photochemistry of flavoprotein light sensors. *Nat Chem Biol*. 2014;10(10):801-809. doi:10.1038/nchembio.1633

88. Lederer F. Extreme pKa displacements at the active sites of FMN-dependent α-hydroxy acid-oxidizing enzymes. *Protein Sci*. 2008;1(4):540-548. doi:10.1002/pro.5560010409

89. Yee EF, Diensthuber RP, Vaidya AT, et al. Signal transduction in light–oxygen–voltage receptors lacking the adduct-forming cysteine residue. *Nat Commun*. 2015;6(1):10079. doi:10.1038/ncomms10079

90. Kaur Grewal R, Mitra D, Roy S. Mapping networks of light–dark transition in LOV photoreceptors. *Bioinformatics*. Published online July 25, 2015:btv429. doi:10.1093/bioinformatics/btv429

91. Albert R, Barabási A-L. Statistical mechanics of complex networks. *Rev Mod Phys*. 2002;74(1):47-97. doi:10.1103/RevModPhys.74.47

92. Brede M. Networks—An Introduction . Mark E. J. Newman. (2010, Oxford University Press.) $65.38, £35.96 (hardcover), 772 pages. ISBN-978-0-19-920665-0. *Artif Life*. 2012;18(2):241-242. doi:10.1162/artl_r_00062

93. Banerjee SJ, Azharuddin M, Sen D, et al. Using complex networks towards information retrieval and diagnostics in multidimensional imaging. *Sci Rep*. 2015;5(1):17271. doi:10.1038/srep17271

94. Roy S. Systems biology beyond degree, hubs and scale-free networks: the case for multiple metrics in complex networks. *Syst Synth Biol*. 2012;6(1-2):31-34. doi:10.1007/s11693-012-9094-y

95. Chennubhotla C, Bahar I. Markov propagation of allosteric effects in biomolecular systems: application to GroEL–GroES. *Mol Syst Biol*. 2006;2(1):36. doi:10.1038/msb4100075

96. Brinda KV, Vishveshwara S. A Network Representation of Protein Structures: Implications for Protein Stability. *Biophys J*. 2005;89(6):4159-4170. doi:10.1529/biophysj.105.064485

97. Deisseroth K. Optogenetics. *Nat Methods*. 2011;8(1):26-29. doi:10.1038/nmeth.f.324

98. OESTERHELT D, STOECKENIUS W. Rhodopsin-like Protein from the Purple Membrane of Halobacterium halobium. *Nat New Biol*. 1971;233(39):149-152. doi:10.1038/newbio233149a0

99. Boyden ES, Zhang F, Bamberg E, Nagel G, Deisseroth K. Millisecond-timescale, genetically targeted optical control of neural activity. *Nat Neurosci*. 2005;8(9):1263-1268. doi:10.1038/nn1525

100. Lanyi JK. Halorhodopsin — a second retinal pigment in Halobacterium halobium. *Trends Biochem Sci*. 1981;6:60-62. doi:10.1016/0968-0004(81)90022-0

101. Nagel G. Channelrhodopsin-1: A Light-Gated Proton Channel in Green Algae. *Science (80-)*. 2002;296(5577):2395-2398. doi:10.1126/science.1072068

102. Aravanis AM, Wang L-P, Zhang F, et al. An optical neural interface: in vivo control of rodent motor cortex with integrated fiberoptic and optogenetic technology. *J Neural Eng*. 2007;4(3):S143-S156. doi:10.1088/1741-2560/4/3/S02

103. Adamantidis AR, Zhang F, Aravanis AM, Deisseroth K, de Lecea L. Neural substrates of awakening probed with optogenetic control of hypocretin neurons. *Nature*. 2007;450(7168):420-424. doi:10.1038/nature06310

104. Strickland D, Moffat K, Sosnick TR. Light-activated DNA binding in a designed allosteric protein. *Proc Natl Acad*

Sci U S A. 2008;105(31):10709-10714. doi:10.1073/pnas.0709610105

105. Wu YI, Frey D, Lungu OI, et al. A genetically encoded photoactivatable Rac controls the motility of living cells. *Nature*. 2009;461(7260):104-108. doi:10.1038/nature08241

106. Kawano F, Suzuki H, Furuya A, Sato M. Engineered pairs of distinct photoswitches for optogenetic control of cellular proteins. *Nat Commun*. 2015;6(1):6256. doi:10.1038/ncomms7256

107. Kyriakakis P, Catanho M, Hoffner N, et al. Biosynthesis of Orthogonal Molecules Using Ferredoxin and Ferredoxin-NADP + Reductase Systems Enables Genetically Encoded PhyB Optogenetics. *ACS Synth Biol*. 2018;7(2):706-717. doi:10.1021/acssynbio.7b00413

108. Uda Y, Goto Y, Oda S, Kohchi T, Matsuda M, Aoki K. Efficient synthesis of phycocyanobilin in mammalian cells for optogenetic control of cell signaling. *Proc Natl Acad Sci*. 2017;114(45):11962-11967. doi:10.1073/pnas.1707190114

109. Ziegler T, MÃ¶glich A. Photoreceptor engineering. *Front Mol Biosci*. 2015;2. doi:10.3389/fmolb.2015.00030

110. Tischer D, Weiner OD. Illuminating cell signalling with optogenetic tools. *Nat Rev Mol Cell Biol*. 2014;15(8):551-558. doi:10.1038/nrm3837

111. Kasahara M, Swartz TE, Olney MA, et al. Photochemical Properties of the Flavin Mononucleotide-Binding Domains of the Phototropins from Arabidopsis, Rice, and Chlamydomonas reinhardtii. *Plant Physiol*. 2002;129(2):762-773. doi:10.1104/pp.002410

112. Wu YI, Frey D, Lungu OI, et al. A genetically encoded photoactivatable Rac controls the motility of living cells. *Nature*. 2009;461(7260):104-108. doi:10.1038/nature08241

113. Pham E, Mills E, Truong K. A Synthetic Photoactivated Protein to Generate Local or Global Ca2+ Signals. *Chem Biol*. 2011;18(7):880-890. doi:10.1016/j.chembiol.2011.04.014

114. Schmidt D, Tillberg PW, Chen F, Boyden ES. A fully genetically encoded protein architecture for optical control of peptide ligand concentration. *Nat Commun*. 2014;5(1):3019. doi:10.1038/ncomms4019

115. Mills E, Chen X, Pham E, Wong S, Truong K. Engineering a Photoactivated Caspase-7 for Rapid Induction of Apoptosis. *ACS Synth Biol*. 2012;1(3):75-82. doi:10.1021/sb200008j

116. Bonger KM, Rakhit R, Payumo AY, Chen JK, Wandless TJ. General Method for Regulating Protein Stability with Light. *ACS Chem Biol*. 2014;9(1):111-115. doi:10.1021/cb400755b

117. Renicke C, Schuster D, Usherenko S, Essen L-O, Taxis C. A LOV2 Domain-Based Optogenetic Tool to Control Protein Degradation and Cellular Function. *Chem Biol*. 2013;20(4):619-626. doi:10.1016/j.chembiol.2013.03.005

118. Yi JJ, Wang H, Vilela M, Danuser G, Hahn KM. Manipulation of Endogenous Kinase Activity in Living Cells Using Photoswitchable Inhibitory Peptides. *ACS Synth Biol*. 2014;3(11):788-795. doi:10.1021/sb5001356

119. Niopek D, Benzinger D, Roensch J, et al. Engineering light-inducible nuclear localization signals for precise

spatiotemporal control of protein dynamics in living cells. *Nat Commun*. 2014;5(1):4404. doi:10.1038/ncomms5404

120. Yumerefendi H, Dickinson DJ, Wang H, et al. Control of Protein Activity and Cell Fate Specification via Light-Mediated Nuclear Translocation. Palazzo AF, ed. *PLoS One*. 2015;10(6):e0128443. doi:10.1371/journal.pone.0128443

121. Dagliyan O, Tarnawski M, Chu P-H, et al. Engineering extrinsic disorder to control protein activity in living cells. *Science (80-).* 2016;354(6318):1441-1444. doi:10.1126/science.aah3404

122. Moon J, Gam J, Lee S-G, Suh Y-G, Lee J. Light-Regulated Tetracycline Binding to the Tet Repressor. *Chem - A Eur J*. 2014;20(9):2508-2514. doi:10.1002/chem.201304027

123. Redchuk TA, Omelina ES, Chernov KG, Verkhusha V V. Near-infrared optogenetic pair for protein regulation and spectral multiplexing. *Nat Chem Biol*. 2017;13(6):633-639. doi:10.1038/nchembio.2343

124. Smart AD, Pache RA, Thomsen ND, Kortemme T, Davis GW, Wells JA. Engineering a light-activated caspase-3 for precise ablation of neurons in vivo. *Proc Natl Acad Sci*. 2017;114(39):E8174-E8183. doi:10.1073/pnas.1705064114

125. Schierling B, Pingoud A. Controlling the DNA Cleavage Activity of Light-Inducible Chimeric Endonucleases by Bidirectional Photoactivation. *Bioconjug Chem*. 2012;23(6):1105-1109. doi:10.1021/bc3001326

126. Spiltoir JI, Strickland D, Glotzer M, Tucker CL. Optical Control of Peroxisomal Trafficking. *ACS Synth Biol*. 2016;5(7):554-560. doi:10.1021/acssynbio.5b00144

127. Wang H, Vilela M, Winkler A, et al. LOVTRAP: an optogenetic system for photoinduced protein dissociation. *Nat Methods*. 2016;13(9):755-758. doi:10.1038/nmeth.3926

128. Westberg M, Bregnhøj M, Etzerodt M, Ogilby PR. No Photon Wasted: An Efficient and Selective Singlet Oxygen Photosensitizing Protein. *J Phys Chem B*. 2017;121(40):9366-9371. doi:10.1021/acs.jpcb.7b07831

129. Yazawa M, Sadaghiani AM, Hsueh B, Dolmetsch RE. Induction of protein-protein interactions in live cells using light. *Nat Biotechnol*. 2009;27(10):941-945. doi:10.1038/nbt.1569

130. Strickland D, Lin Y, Wagner E, et al. TULIPs: tunable, light-controlled interacting protein tags for cell biology. *Nat Methods*. 2012;9(4):379-384. doi:10.1038/nmeth.1904

131. Lungu OI, Hallett R a., Choi EJ, Aiken MJ, Hahn KM, Kuhlman B. Designing Photoswitchable Peptides Using the AsLOV2 Domain. *Chem Biol*. 2012;19(4):507-517. doi:10.1016/j.chembiol.2012.02.006

132. Guntas G, Hallett RA, Zimmerman SP, et al. Engineering an improved light-induced dimer (iLID) for controlling the localization and activity of signaling proteins. *Proc Natl Acad Sci*. 2015;112(1):112-117. doi:10.1073/pnas.1417910112

133. Giraldo R. Optogenetic Navigation of Routes Leading to Protein Amyloidogenesis in Bacteria. *J Mol Biol*. 2019;431(6):1186-1202. doi:10.1016/j.jmb.2019.01.037

134. Lee CT, Malzahn E, Brunner M, Mayer MP. Light-induced differences in conformational dynamics of the circadian clock regulator VIVID. *J Mol Biol*. 2014;426(3):601-610. doi:10.1016/j.jmb.2013.10.035

135. French AR, Sosnick TR, Rock RS. Investigations of human myosin VI targeting using optogenetically controlled cargo loading. *Proc Natl Acad Sci*. 2017;114(9):E1607-E1616. doi:10.1073/pnas.1614716114

136. Cosentino C, Alberio L, Gazzarrini S, et al. Engineering of a light-gated potassium channel. *Science (80-)*. 2015;348(6235):707-710. doi:10.1126/science.aaa2787

137. Papanatsiou M, Petersen J, Henderson L, Wang Y, Christie JM, Blatt MR. Optogenetic manipulation of stomatal kinetics improves carbon assimilation, water use, and growth. *Science (80-)*. 2019;363(6434):1456-1459. doi:10.1126/science.aaw0046

138. Wang W, Wildes CP, Pattarabanjird T, et al. A light- and calcium-gated transcription factor for imaging and manipulating activated neurons. *Nat Biotechnol*. 2017;35(9):864-871. doi:10.1038/nbt.3909

139. Peter E, Dick B, Baeurle SA. Mechanism of signal transduction of the LOV2-Jα photosensor from Avena sativa. *Nat Commun*. 2010;1(1):122. doi:10.1038/ncomms1121

140. Jones MA, Feeney KA, Kelly SM, Christie JM. Mutational Analysis of Phototropin 1 Provides Insights into the Mechanism Underlying LOV2 Signal Transmission. *J Biol Chem*. 2007;282(9):6405-6414. doi:10.1074/jbc.M605969200

141. Nozaki D, Iwata T, Ishikawa T, Todo T, Tokutomi S, Kandori H. Role of Gln1029 in the Photoactivation Processes of the LOV2 Domain in Adiantum Phytochrome3 †. *Biochemistry*. 2004;43(26):8373-8379. doi:10.1021/bi0494727

142. Freddolino PL, Dittrich M, Schulten K. Dynamic Switching Mechanisms in LOV1 and LOV2 Domains of Plant Phototropins. *Biophys J*. 2006;91(10):3630-3639. doi:10.1529/biophysj.106.088609

143. Nash AI, Mcnulty R, Elizabeth M, Swartz TE, Bogomolni RA, Luecke H. Correction for Nash et al., Structural basis of photosensitivity in a bacterial light-oxygen-voltage/helix-turn-helix (LOV-HTH) DNA-binding protein. *Proc Natl Acad Sci*. 2012;109(15):5904-5904. doi:10.1073/pnas.1204100109

144. Grosdidier A, Zoete V, Michielin O. SwissDock, a protein-small molecule docking web service based on EADock DSS. *Nucleic Acids Res*. 2011;39(suppl):W270-W277. doi:10.1093/nar/gkr366

145. Schumacher JM, Ellias SA, Palmer EP, et al. Transplantation of embryonic porcine mesencephalic tissue in patients with PD. *Neurology*. 2000;54(5):1042-1050. doi:10.1212/WNL.54.5.1042

146. Schwede T. SWISS-MODEL: an automated protein homology-modeling server. *Nucleic Acids Res*. 2003;31(13):3381-3385. doi:10.1093/nar/gkg520

147. Kabsch W. A solution for the best rotation to relate two sets of vectors. *Acta Crystallogr Sect A*. 1976;32(5):922-923. doi:10.1107/S0567739476001873

148. Chen VB, Arendall WB, Headd JJ, et al. MolProbity : all-atom structure validation for macromolecular

crystallography. *Acta Crystallogr Sect D Biol Crystallogr*. 2010;66(1):12-21. doi:10.1107/S0907444909042073

149. Deb A, Kaur Grewal R, Roy S, Mitra D. Residue Interaction Dynamics in *Vaucheria* Aureochrome1 LOV : Bridging Theory and Experiments. *Proteins Struct Funct Bioinforma*. Published online July 18, 2020:prot.25984. doi:10.1002/prot.25984

150. Zayner JP, Sosnick TR. Factors that control the chemistry of the LOV domain photocycle. *PLoS One*. 2014;9(1). doi:10.1371/journal.pone.0087074

151. Raffelberg S, Mansurova M, Gärtner W, Losi A. Modulation of the Photocycle of a LOV Domain Photoreceptor by the Hydrogen-Bonding Network. *J Am Chem Soc*. 2011;133(14):5346-5356. doi:10.1021/ja1097379

152. Ito S, Song YH, Imaizumi T. LOV Domain-Containing F-Box Proteins: Light-Dependent Protein Degradation Modules in Arabidopsis. *Mol Plant*. 2012;5(3):573-582. doi:10.1093/mp/sss013

153. Zoltowski BD, Vaccaro B, Crane BR. Mechanism-based tuning of a LOV domain photoreceptor. *Nat Chem Biol*. 2009;5(11):827-834. doi:10.1038/nchembio.210

154. Heintz U, Schlichting I. Blue light-induced LOV domain dimerization enhances the affinity of Aureochrome 1a for its target DNA sequence. *Elife*. 2016;5. doi:10.7554/eLife.11860

155. Banerjee A, Herman E, Kottke T, Essen L-O. Structure of a Native-like Aureochrome 1a LOV Domain Dimer from Phaeodactylum tricornutum. *Structure*. 2016;24(1):171-178. doi:10.1016/j.str.2015.10.022

156. Micsonai A, Wien F, Kernya L, et al. Accurate secondary structure prediction and fold recognition for circular dichroism spectroscopy. *Proc Natl Acad Sci*. 2015;112(24):E3095-E3103. doi:10.1073/pnas.1500851112

157. Kabsch W, Sander C. Dictionary of protein secondary structure: Pattern recognition of hydrogen-bonded and geometrical features. *Biopolymers*. 1983;22(12):2577-2637. doi:10.1002/bip.360221211

158. Hart JE, Sullivan S, Hermanowicz P, et al. Engineering the phototropin photocycle improves photoreceptor performance and plant biomass production. *Proc Natl Acad Sci*. 2019;116(25):12550-12557. doi:10.1073/pnas.1902915116

Devrani Mitra <devrani.dbs@presiuniv.ac.in>

[Urkund] 1% similarity - devrani.dbs@presiuniv.ac.in

1 message

report@analysis.urkund.com <report@analysis.urkund.com> Fri, Oct 16, 2020 at 12:50 PM
To: devrani.dbs@presiuniv.ac.in

Document sent by: devrani.dbs@presiuniv.ac.in
Document received: 10/16/2020 9:19:00 AM
Report generated 10/16/2020 9:20:45 AM by Urkund's system for automatic control.

Student message: Please find the document attached for plagiarism check.

Thanks and regards,
Devrani

--
Dr. Devrani Mitra
Assistant Professor (Stage II)
Dept. of Life Sciences
Presidency University
86/1 College Street,
Kolkata 700073 WB India

Web: https://sites.google.com/site/devranimitra/
https://www.presiuniv.ac.in/web/staff.php?staffid=66

Document : 5000 only word.docx [D81828107]

IMPORTANT! The analysis contains 1 warning(s).

About 1% of this document consists of text similar to text found in 86 sources. The largest marking is 13 words long and is 100% similar to its primary source.

PLEASE NOTE that the above figures do not automatically mean that there is plagiarism in the document. There may be good reasons as to why parts of a text also appear in other sources. For a reasonable suspicion of academic dishonesty to present itself, the analysis, possibly found sources and the original document need to be examined closely.

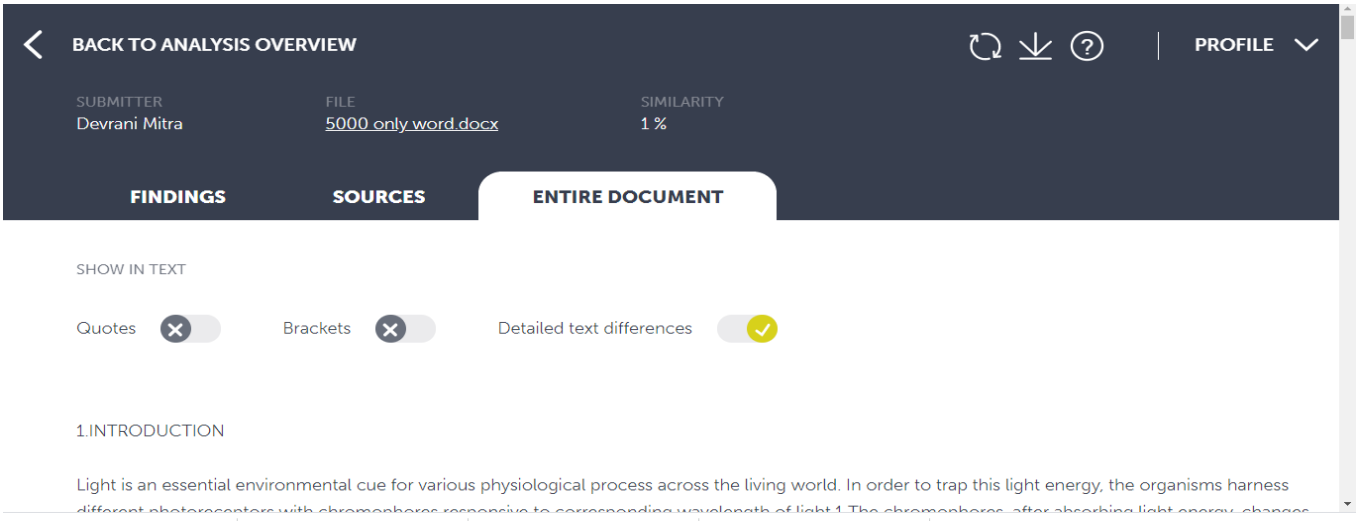

Conferences attended and workshops attended:

1. **Indo-US conference on Synthetic and Systems Biology, 2014. Hosted by Jawaharlal Nehru University, New Delhi.**
2. **National Symposium on "Molecules to systems", 2015. Organized and Hosted by Presidency University.**
3. **International Biological Engineering Meeting, 2017. Hosted Jawaharlal Nehru University, New Delhi.**
4. **CSIR-IICB Skill Development Program, 2019 for Small Molecule Crystallography.**
5. **Conference on Recent Advances in Metabolic Engineering for Microbial Cell Factories, 2020. Organized by Indian Institute of Technology, Kharagpur.**

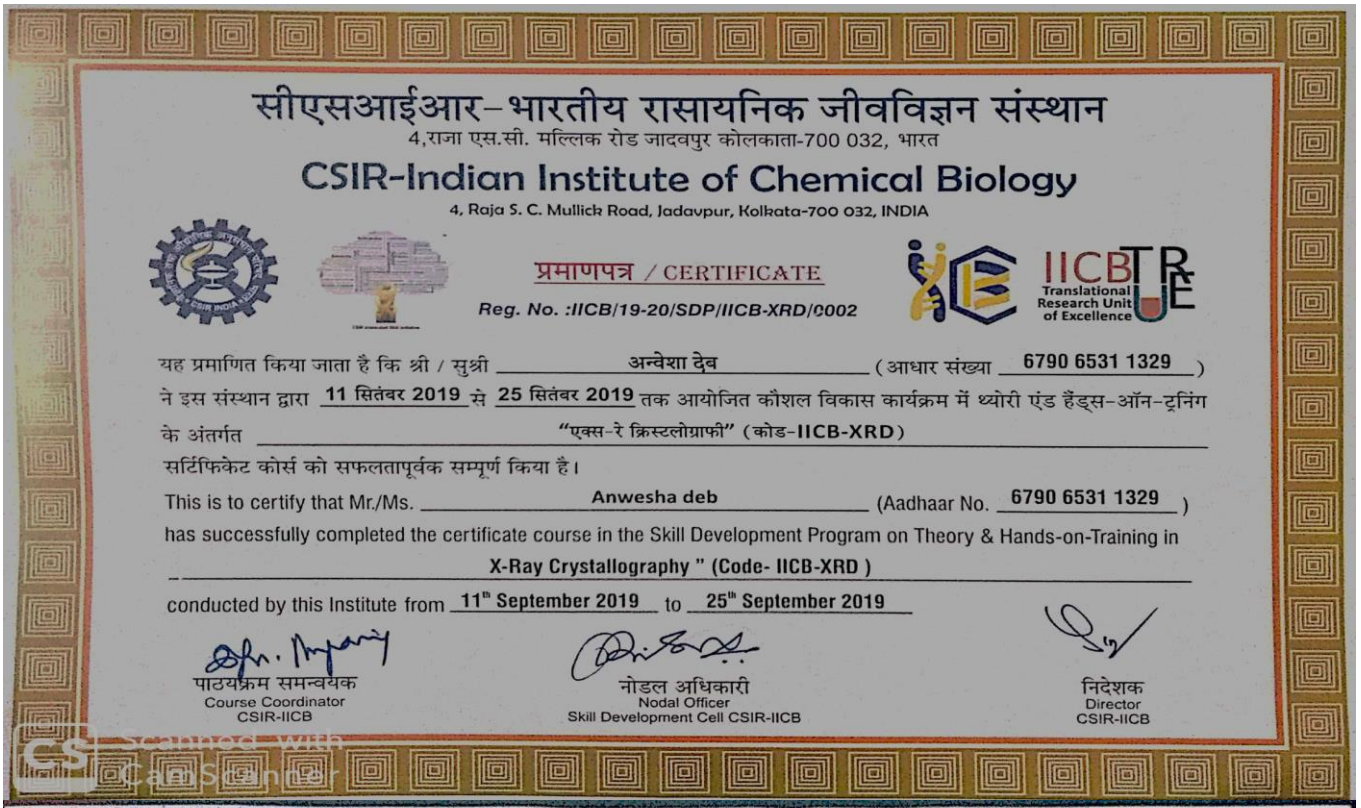

सीएसआईआर–भारतीय रासायनिक जीवविज्ञन संस्थान
4,राजा एस.सी. मल्लिक रोड जादवपुर कोलकाता-700 032, भारत

CSIR-Indian Institute of Chemical Biology
4, Raja S. C. Mullick Road, Jadavpur, Kolkata-700 032, INDIA

IICB Translational Research Unit of Excellence

प्रमाणपत्र / CERTIFICATE

Reg. No. :IICB/19-20/SDP/IICB-XRD/0002

यह प्रमाणित किया जाता है कि श्री / सुश्री अन्वेशा देब (आधार संख्या 6790 6531 1329)
ने इस संस्थान द्वारा 11 सितंबर 2019 से 25 सितंबर 2019 तक आयोजित कौशल विकास कार्यक्रम में थ्योरी एंड हैंड्स-ऑन-ट्रेनिंग
के अंतर्गत "एक्स-रे क्रिस्टलोग्राफी" (कोड-IICB-XRD)
सर्टिफिकेट कोर्स को सफलतापूर्वक सम्पूर्ण किया है।

This is to certify that Mr./Ms. Anwesha deb (Aadhaar No. 6790 6531 1329)
has successfully completed the certificate course in the Skill Development Program on Theory & Hands-on-Training in
X-Ray Crystallography " (Code- IICB-XRD)
conducted by this Institute from 11th September 2019 to 25th September 2019

पाठ्यक्रम समन्वयक
Course Coordinator
CSIR-IICB

नोडल अधिकारी
Nodal Officer
Skill Development Cell CSIR-IICB

निदेशक
Director
CSIR-IICB

Scanned with CamScanner

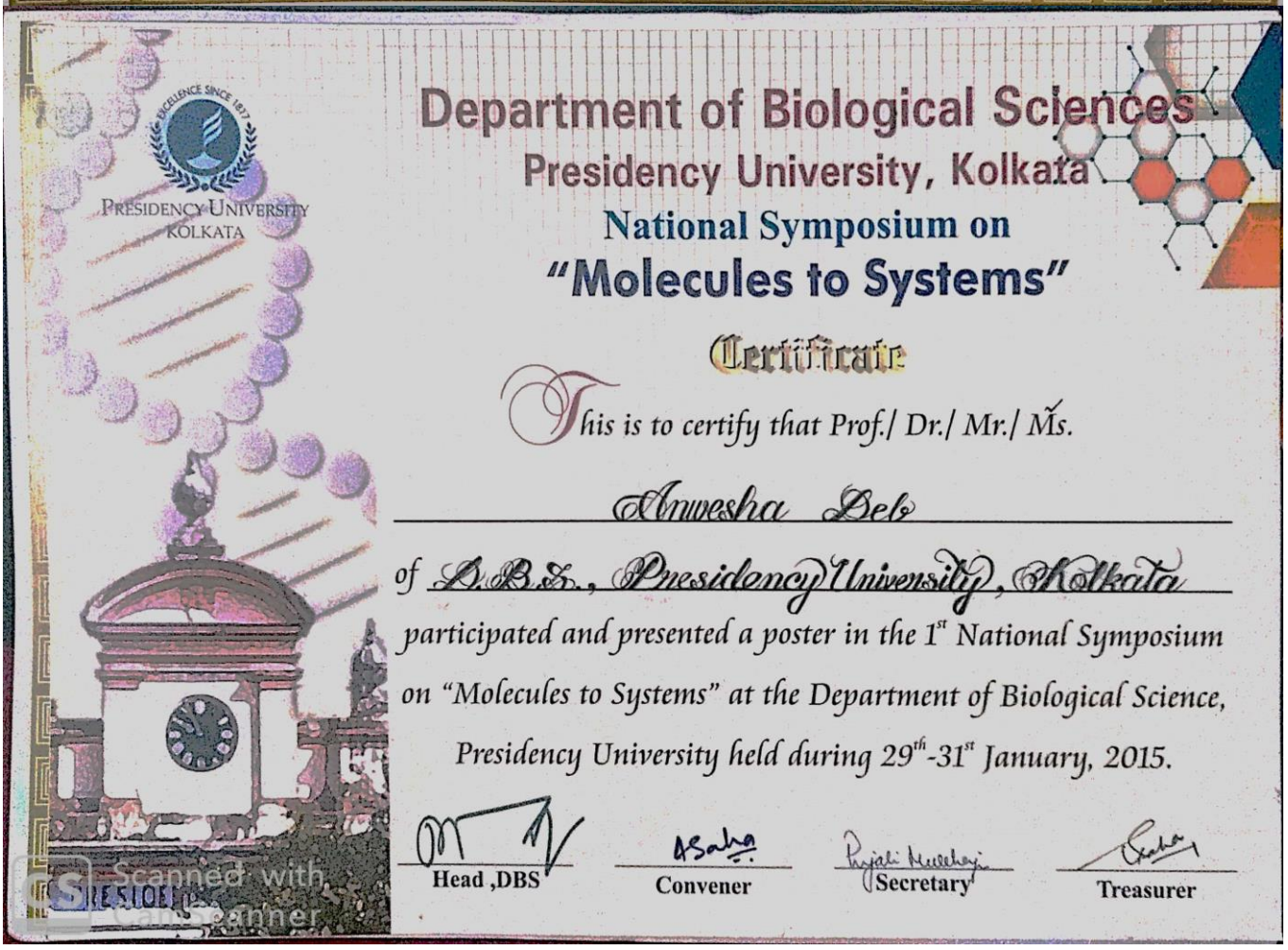

PRESIDENCY UNIVERSITY
KOLKATA

Department of Biological Sciences
Presidency University, Kolkata
National Symposium on
"Molecules to Systems"

Certificate

This is to certify that Prof./ Dr./ Mr./ Ms.

Anwesha Deb

of D.B.S., Presidency University, Kolkata

participated and presented a poster in the 1st National Symposium on "Molecules to Systems" at the Department of Biological Science, Presidency University held during 29th-31st January, 2015.

Head ,DBS | Convener | Secretary | Treasurer

Scanned with CamScanner

Received: 30 March 2020 | Revised: 4 June 2020 | Accepted: 12 July 2020
DOI: 10.1002/prot.25984

RESEARCH ARTICLE

PROTEINS WILEY

Residue interaction dynamics in *Vaucheria* aureochrome1 light-oxygen-voltage: Bridging theory and experiments

Anwesha Deb[1] | Rajdeep Kaur Grewal[2] | Soumen Roy[2] | Devrani Mitra[1]

[1]Department of Life Sciences, Presidency University, Kolkata, India

[2]Department of Physics, Bose Institute, Kolkata, India

Correspondence
Soumen Roy, Department of Physics, Bose Institute, 93/1 APC Road, Kolkata 70009, India.
Email: soumen@jcbose.ac.in

Devrani Mitra, Department of Life Sciences, Presidency University, 86/1 College Street, Kolkata 700073, India.
Email: devrani.dbs@presiuniv.ac.in

Funding information
Department of Biotechnology, Ministry of Science and Technology, Grant/Award Number: BT/PR26435/BRB/10/1627/2017; Science and Engineering Research Board, Grant/Award Number: EMR/2015/000144

Abstract

Allosteric communication is the basis of signaling and information transfer. Collective interactions between amino acid residues, which are spatially distributed in the three dimensional structure of a protein molecule, form the basis of allosteric network. While the construction of residue interaction graphs (RIG) is based on static crystal structures of proteins, it is important to extract information on protein dynamics to understand allostery. Therefore, quantitative analysis of RIG based on the framework of differential network (DN), is immensely helpful in identifying key amino acid residue interactions within such communication pathways. While the simultaneous availability of protein structures from two different states is essential for DN, there are additional challenges. Crystallographic artifacts like nonbiological dimeric arrangements within the crystal lattice automatically influence the construction and eventually the interpretation of RIG. Therefore, experimental validation of predictions from the analyses of RIG is naturally scarce in the literature. Herein, we study the photo sensor domain of the signaling photoreceptor transcription factor, aureochrome1, to understand light-driven signaling. We perform direct experiments to verify the predictions from RIG using the machinery of DN. However, the agreement leaves scope for improvement. We then discuss the notion of quaternary structure alignment to obtain a biologically meaningful dimer. Thence, we reconstruct the RIG and reanalyze the modified structure. Results of these reanalyses render far superior agreement with experiments. Therefore, this notion of addressing crystallographic biases provides a fresh yet general approach for reconciliation of theory and experiments. It is applicable beyond the present case to all signaling proteins in general.

KEYWORDS
aureochrome1 LOV, dark recovery kinetics, residue interaction dynamics, residue interaction graph, signaling

1 | INTRODUCTION

The importance of topology is widely appreciated across the sciences. In chemistry, immense knowledge can be obtained from a molecular graph or structural formula. In biochemistry, the biochemical reaction network theory analyses complex biochemical reaction networks in terms of the emergent features of their topology. Structure-function relations in a protein including allosteric interactions have been widely studied using energetics and statistical mechanical concepts.[1] However, it is equally well known that these are computationally expensive. Parallelly, in recent years, intense activity has centered on approaches drawn from graph theory and network science.[2,3] Herein, residue interaction graphs (RIG) are obtained from the three-dimensional crystal structure of a given protein and biologically